Tim Gregorčič*, Stevan Savić**, Blaž Repe*,
Matej Ogrin*

KARTIRANJE LOKALNIH PODNEBNIH OBMOČIJ LJUBLJANE: DVOJNI METODOLOŠKI PRISTOP

COBISS 1.01
DOI: 10.4312/GRKP6310

Izvleček

Sistem lokalnih podnebnih območij (LPO) je bil zasnovan za omogočanje standardiziranega raziskovalnega pristopa na področju mestne klimatologije in sorodnih znanstvenih disciplin. V tej študiji je predstavljena klasifikacija LPO Ljubljane, za kar sta bili uporabljeni metodi celičnega avtomata in WUDAPT. Ustreznost klasifikacij je bila ovrednotena glede na zmožnost identifikacije prostorskih razlik v temperaturi površja in prizemnega mestnega toplotnega otoka ter s strokovno presojo. Klasifikacija metode WUDAPT velja za bolj reprezentativno in predstavlja podlago za nadaljnje podnebne študije Ljubljane.

Ključne besede: lokalna podnebna območja (LPO), metoda WUDAPT, metoda celičnega avtomata (CA), mestno podnebje, mikrometeorološka klasifikacija

*Oddelek za geografijo, Filozofska fakulteta Univerze v Ljubljani, Aškerčeva 2, SI-1000 Ljubljana, Slovenija
**Oddelek za geografijo, turizem in hotelirstvo, Fakulteta za naravoslovje, Univerza v Novem Sadu, Trg Dositeja Obradovića 3, RS-21000 Novi Sad, Srbija
e-pošta: tim.gregorcic@ff.uni-lj.si; stevan.savic@dgt.uns.ac.rs, blaz.repe@ff.uni-lj.si, matej.ogrin@ff.uni-lj.si
ORCID: 0009-0006-9767-9428 (T. Gregorčič), 0000-0002-4297-129X (S. Savić), 0000-0002-5530-4840 (B. Repe), 0000-0002-4742-3890 (M. Ogrin)

1 UVOD

Do sredine 21. stoletja lahko pričakujemo, da bo več kot 60 % svetovnega prebivalstva živelo v mestih (Združeni narodi, 2019). Čeprav ne gre pričakovati, da bo urbanizacija v večini evropskih držav primerljiva urbanizaciji številnih držav globalnega juga, to ne pomeni nujno manj urbanih izzivov. Evropska mesta so še vedno smiseln predmet proučevanja z več vidikov zaradi nastajajočih težav, povezanih s podnebnimi in drugimi okoljskimi spremembami, staranjem prebivalstva, tehnološkim napredkom in družbenimi neenakostmi. Ker je podnebje eden od najpomembnejših dejavnikov kakovosti življenja, so študije mestnega podnebja bistvenega pomena za razvoj mest prihodnosti z ugodnimi življenjskimi pogoji. Urbanopodnebne študije se pogosto osredotočajo na teme, kot so kakovost zraka (Qian in sod., 2025), notranja in zunanja toplotna obremenitev ljudi (Hu in sod., 2023; Mohite in Surawar, 2024), mestni toplotni otok (MTO) (Assaf in Assaad, 2024; Ogrin, 2015; Ogrin in Krevs, 2015; Ogrin in sod., 2023; Pipenbaher in sod., 2020; Žiberna, 2006; Žiberna in Ivajnšič, 2022) in lokalna podnebna območja (LPO) (Ogrin in sod., 2022; Wang in sod., 2024; Žiberna in sod., 2021). LPO sta opredelila Stewart in Oke (2012, str. 1884) kot »območja s homogeno rabo tal, strukturo, materiali in človekovimi dejavnostmi, ki se horizontalno raztezajo od nekaj sto metrov do več kilometrov«. Klasifikacija LPO vključuje 10 pretežno pozidanih in 7 pretežno naravnih tipov, pri čemer je za vsak tip značilna posebna prostorska morfologija in pokrovnost (slika 1). Čeprav to ni edini način urbanopodnebne conacije, je le-ta najpogosteje uporabljen in zato uveljavljen kot standard v študijah mestnega podnebja (Lehnert in sod., 2021). LPO niso zgolj predmet raziskav *per se*, temveč pogosto tudi podlaga za analizo prostorske dinamike drugih urbanih pojavov. Posledično je razvoj zanesljive klasifikacije LPO za poselitvene centre ključnega pomena, saj so lahko podlaga za aplikativne urbanopodnebne študije, katerih cilj je povečati odpornost mest proti posledicam podnebnih sprememb, posebno proti zunanji toplotni obremenitvi ljudi v času vročega vremena.

V preteklosti je bilo razvitih več klasifikacijskih metod, ki jih razvrščamo v 4 glavne skupine. To so klasifikacije, ki temeljijo na (a) metodah daljinskega zaznavanja, (b) geoinformacijskih metodah, (c) integraciji metod daljinskega zaznavanja in geoinformatike in (d) strokovni presoji (Lehnert in sod., 2021). Pristopi, ki temeljijo na metodah daljinskega zaznavanja, klasificirajo LPO z metodami nadzorovane klasifikacije in uporabo satelitskih posnetkov ter drugih daljinsko zaznanih podatkov. Metode te skupine so najpogosteje uporabljene, med njimi pa je najbolj priljubljena metoda WUDAPT (Huang in sod., 2023). Metoda WUDAPT (ang. *World Urban Database and Access Portal Tools*) je bila razvita v sklopu istoimenskega projekta, katerega cilj je bil omogočiti pridobivanje, shranjevanje in deljenje globalnih urbanih podnebnih podatkov (Mills in sod., 2015). Med drugim omogoča klasifikacijo LPO z uporabo algoritmov naključnih gozdov in satelitskih posnetkov. Ta metoda je bila npr. uporabljena za klasifikacijo LPO Pariza, Milana in Londona (Qiu in sod., 2019).

Slika 1: Opis lokalnih podnebnih območij.

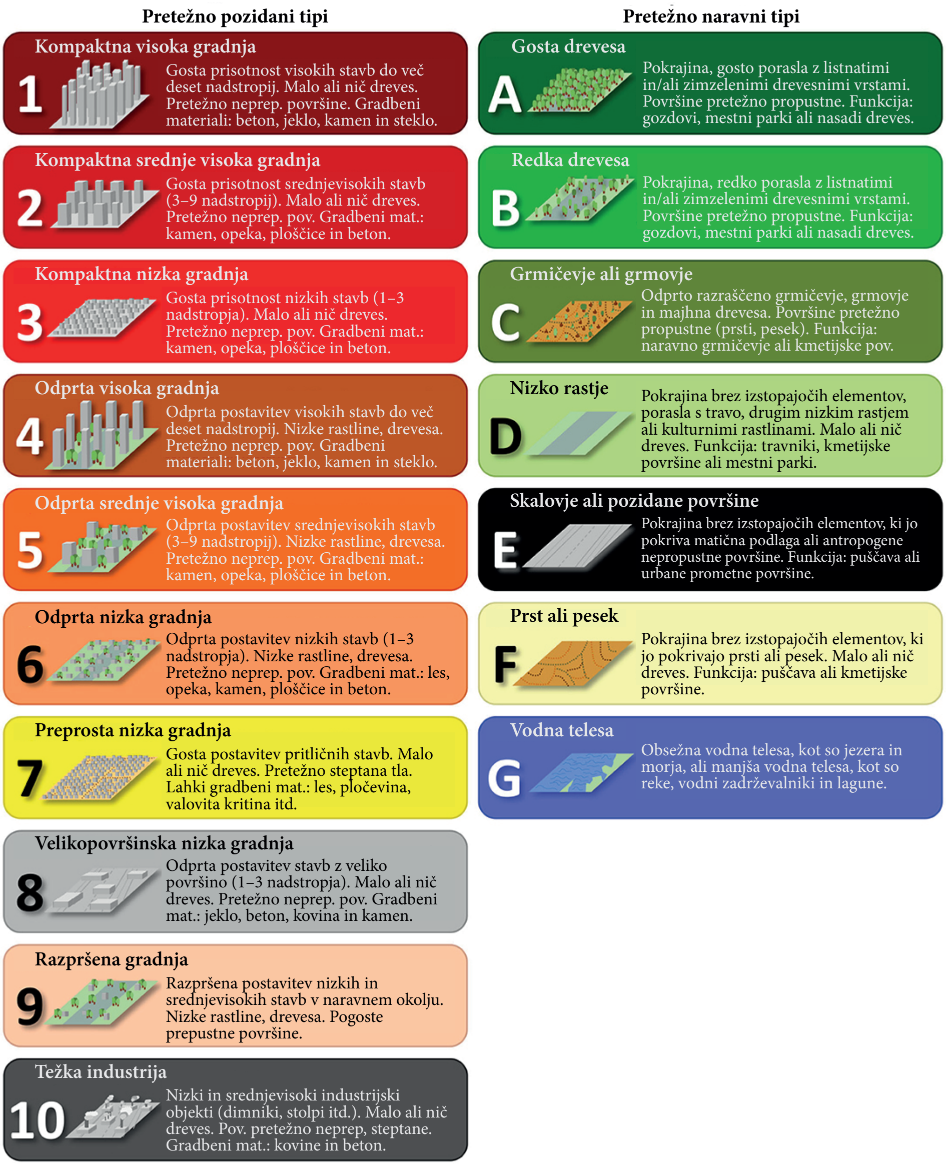

Vir: Demuzere in sod., 2021.

Klasifikacijski pristopi, ki temeljijo na geoinformacijskih metodah, določajo LPO z izračunom njihovih fizičnih parametrov, opredelitvijo prostorske ločljivosti klasifikacije in ovrednotenjem njene kakovosti (Huang in sod., 2023). Primer tega pristopa je klasifikacija LPO Segedina (Unger in sod., 2014).

Z integriranimi pristopi, ki združujejo metode daljinskega zaznavanja in geoinformatike, se lahko izognemo oviram, ki jih predstavljajo manjkajoči podatki o fizičnih parametrih ali rabi tal. Ustvarimo lahko klasifikacije, ki so alternativa klasifikacijam prve ali druge metodološke skupine, in v primerjavi z metodami prve skupine izboljšamo sposobnost upoštevanja razlik v morfologiji mesta in rabi tal na najnižjih prostorskih ravneh (Lehnert in sod., 2021). Zhou in sod. (2020) so tovrstni pristop uporabili za klasifikacijo LPO mesta Sendai.

Metode, ki temeljijo na strokovni presoji, se opirajo na lokalno metapodatkovno znanje strokovnjakov o meteoroloških postajah urbane meteorološke mreže, ki predstavljajo različne mikro ali lokalne pogoje. Ker so urbane meteorološke mreže redke, se redko uporabljajo tudi te metode (Lehnert in sod., 2021). Primer je študija, izvedena v Novem Sadu, kjer je bilo devet LPO opredeljenih kot potencialne lokacije za 28 prihodnjih mestnih meteoroloških postaj (Savić in sod., 2013). Podobno je bil ta pristop uporabljen pri klasifikaciji LPO mesta Olomouc (Lehnert in sod., 2015).

Čeprav so bile klasifikacije LPO izvedene za številna mesta Srednje in Jugovzhodne Evrope, poglobljena študija LPO v Ljubljani še ni bila opravljena. Ljubljana ima sicer več kot 20-letno zgodovino proučevanja mestnega toplotnega otoka (MTO). Prva obsežnejša študija pojava datira že v leto 2000 (Jernej, 2000), ko so bile uveljavljene metode določevanja MTO, drugačne od današnjih. Ciglič in Komac (2014) sta se lotila daljinskega zaznavanja MTO v Ljubljani in s sodelavci pripravila Atlas MTO srednjeevropskih mest, v letih 2020–2022 pa je Oddelek za geografijo UL FF izvedel obsežnejšo študijo MTO v Ljubljani. Vključili so terenske meritve, mrežo stacionarnih meteoroloških postaj in satelitske posnetke ter med drugim določili tudi »lokalna temperaturna območja« (LTO) (Ogrin in sod., 2022). LTO deloma izvirajo iz LPO, a je metodologija njihove določitve le delno sledila metodologiji Stewarta in Oka (2012). Posledično LTO ne moremo enačiti z LPO niti jih primerjati s podobnimi tujimi študijami. Ker je bila ta vrzel prisotna še v mnogih drugih mestih po svetu, so Demuzere in sod. (2022) uporabili metodo WUDAPT za izdelavo globalnega sloja LPO. V njihovo študijo je bila sicer vključena tudi Ljubljana, vendar so bili rezultati za pretežno pozidane tipe (LPO 1–10) preveč posplošeni zaradi pomanjkanja *in-situ* opredeljenih učnih območij v Ljubljani. Poleg tega rezultati niso bili ovrednoteni z vidika zmožnosti razlage prostorskih razlik urbanih podnebnih parametrov, kot sta MTO in temperatura površja (TP).

Namen naše raziskave je bil zato klasificirati LPO Ljubljane glede na opredelitev Stewarta in Oka (2012). Cilji so bili: (C1) ustvariti prostorske podatke, potrebne za klasifikacijo LPO, (C2) klasificirati LPO Ljubljane z uporabo metode celičnega avtomata (CA), (C3) klasificirati LPO Ljubljane z uporabo metode WUDAPT in (C4) ovrednotiti rezultate obeh metodologij na podlagi njune sposobnosti pojasnjevanja prostorske spremenljivosti TP in prizemnega MTO ter na podlagi strokovne presoje avtorjev.

2 METODOLOGIJA

2.1 Izdelava vhodnih podatkovnih slojev

Proučevano območje je bilo definirano glede na meje naselja Ljubljana, kot ga v registru prostorskih enot definira Geodetska uprava Republike Slovenije (GURS, 2023b). Če ni navedeno drugače, so bili vhodni podatki za klasifikacijo ustvarjeni z uporabo programskega orodja ArcGIS Pro. Podatkovni sloji, ki smo jih ustvarili, so:

- delež nepozidanih površin na celico (DNP),
- delež stavbnih površin na celico (DSP),
- delež drugih pozidanih površin na celico (DPP),
- delež vidnega neba na celico (DVN),
- višina elementov hrapavosti površja (VEHP),
- razmerje med višino objektov in širino med njimi (RVŠ),
- razredi hrapavosti površja (RHP) in
- albedo površja (AP).

Delež nepozidanih površin na celico: Sloj deleža nepozidanih površin na celico (razmerje med prepustnimi površinami v celici in površino celice v %) je bil ustvarjen z uporabo več podatkovnih virov. Iz rdečih, zelenih, modrih in bližnje infrardečih (NIR) spektralnih ortofoto posnetkov iz leta 2015 smo ustvarili kompozitni sloj (GURS, 2015). Kompozitni sloj smo uporabili kot vhodni podatek za nadzorovano klasifikacijo pozidanih in nepozidanih površin z uporabo metode nadzorovane klasifikacije s pomočjo klasifikacijskega orodja ArcGIS Pro. Dodatno smo iz podatkov rdečega in NIR spektra izračunali sloj NDVI (Goward in sod., 1991) in zvezne vrednosti pretvorili v dva razreda: območja, porasla z rastlinstvom (NDVI ≥ 0,2), in ostala območja (NDVI < 0,2). Razred nepozidanih površin nadzorovane klasifikacije in razred zelenih površin sloja NDVI smo združili s kategorijami vektorskega sloja rabe tal (MKGP, 2023), ki so prikazane v preglednici 1. Združeni sloj je vseboval vse prepustne in neprepustne površine proučevanega območja. Kakovost klasifikacije je bila ocenjena s Cohenovim koeficientom kappa (Olofsson in sod., 2014), ki je znašal 0,93. Glede na ta rezultat smo ocenili, da se klasifikacija skoraj popolno sklada z dejanskim stanjem (Chien-Ta in sod., 2015). V naslednjem koraku je bila ustvarjena poligonalna mreža z dolžino stranic 100 m, ki je predstavljala prostorsko ločljivost klasifikacije LPO z uporabo metode CA. Prostorsko ločljivost smo določili po zgledu sorodnih študij (Demuzere in sod., 2021; Geletič in Lehnert, 2016; Huang in sod., 2023; Kim in sod., 2021). Vsakemu poligonu je bila nato dodeljena izračunana vrednost deleža nepozidanih površin.

Preglednica 1: Razredi sloja rabe tal, ki so bili uporabljeni za prepoznavanje neprepustnih površin.

Šifra	Poimenovanje	Šifra	Poimenovanje	Šifra	Poimenovanje
1100	njiva	1240	ostali trajni nasadi	1600	neobdelano kmetijsko zemljišče
1180	trajne rastline na njivskih površinah	1300	trajni travniki	1800	kmetijsko zemljišče, poraslo z gozdnim drevjem
1211	vinogradi	1321	barjanski travniki	2000	gozd
1212	matičnjaki	1410	kmetijsko zemljišče v zaraščanju	4220	ostalo zamočvirjeno zemljišče
1221	intenzivni sadovnjaki	1420	plantaža gozdnega drevja	7000	voda
1222	ekstenzivni oziroma travniški sadovnjaki	1500	drevesa in grmičevja		

Vir: MKGP, 2023.

Delež stavbnih površin na celico: Sloj deleža stavbnih površin na celico (razmerje med stavbnimi površinami v celici in površino celice v %) je temeljil na sloju katastra nepremičnin (KNP) (GURS, 2023a). V poznejših fazah metodologije so bili uporabljeni lidarski podatki, zajeti med letoma 2014 in 2015 (ARSO, 2011). Za zagotovitev primerljivosti KNP in lidarskih podatkov so bile iz sloja KNP izključene vse stavbe, zgrajene po letu 2015. Iz podatkov LiDAR smo v prostorski ločljivosti 1 m ustvarili normalizirani digitalni model površja (nDMP) in izračunali povprečno višino nepremičnin. Poligoni s povprečno višino 2,5 m ali manj so bili odstranjeni. V nekaterih primerih je nDMP še vedno vključeval višine stavb, ki so bile porušene po letu 2015, a jih KNP ni vključeval. Ker so bili takšni primeri redki, smo to napako zanemarili. V naslednjem koraku smo izračunali skupno površino nepremičnin vsakega poligona, glede na to pa delež stavbnih površin.

Delež drugih pozidanih površin na celico: Po izdelavi slojev deležev nepozidanih in stavbnih površin na celico smo sloj deleža drugih pozidanih površin na celico (razmerje med neprepustnimi površinami v celici, med katere ne spadajo stavbne površine, in površino celice v %) izračunali s formulo 1.

Formula 1: DPP = 100 – DNP – DSP

Delež vidnega neba na celico: Za sloj deleža vidnega neba na celico (razmerje med vidnim delom nebesne poloble z nivoja tal in celotno nezastrto poloblo) smo ustvarili nDMP, ki je vseboval podatke o višinah površja, visokega rastlinstva in stavb. Sloj je bil ustvarjen iz lidarskih podatkov v prostorski ločljivosti 1 m. Delež vidnega neba na celico je bil nato izračunan iz ustvarjenega sloja z orodjem *Sky View Factor* programske opreme SAGA GIS. Iz surovega sloja deleža vidnega neba smo ustvarili filtrirani sloj tako, da smo odstranili vsa območja, ki so prostorsko sovpadala z območji nDMP z vrednostjo višjo od 0 m. Na koncu smo za vsak poligon mreže izračunali povprečno vrednost deleža vidnega neba filtriranega sloja.

Višina elementov hrapavosti površja: Sloj višine elementov hrapavosti površja vključuje vse elemente prostora z višino. Kadar je bil delež nepozidanih površin na celico manjši od 90 %, delež drugih pozidanih površin na celico pa hkrati med 90 in 10 %, smo upoštevali višine stavb. Kadar je delež nepozidanih površin na celico znašal 90 % ali več ali kadar je delež drugih pozidanih površin znašal 90 % ali več, smo upoštevali višino celotne vegetacije, ne zgolj dreves (Stewart in Oke, 2012). Za podatke o višinah stavb je bil uporabljen sloj nDMP, ustvarjen za izračun deleža drugih pozidanih površin na celico. Za višino vse vegetacije je bil ustvarjen nov sloj nDMP iz kategorij lidarskih podatkov za površje, nizko, srednje visoko in visoko vegetacijo. Na podlagi opisane Boolove logike je bila za vsak poligon v mreži izračunana povprečna vrednost ustreznega nDMP brez upoštevanja celic z vrednostjo 0 m.

Razmerje med višino objektov in širino med njimi: Razmerje med višino objektov in širino med njimi je opredeljeno kot povprečno razmerje med višino in širino uličnih kanjonov ali razmikov med stavbami (kjer je delež nepozidanih površin na celico manjši od 90 %, delež drugih pozidanih površin na celico pa hkrati med 90 in 10 %) ali razmikov med drevesi (kjer delež nepozidanih površin na celico znaša 90 % ali več ali kadar znaša delež drugih pozidanih površin 90 % ali več) (Stewart in Oke, 2012). Podatki o višinah stavb in dreves so že bili na voljo, izračunati pa je bilo treba še širino prostora med njimi. V ta namen so bila iz poligonske mreže izključena vektorizirana območja stavb ali krošenj dreves. Z uporabo vtičnika za ArcGIS Pro, imenovanega XTools Pro, je bila z orodjem *Polygon Width* izračunana povprečna širina vmesnega prostora. Točkovni rezultati so bili nato povprečeni glede na poligonsko mrežo, kar je omogočilo izračun razmerja med višino objektov in širino med njimi.

Razredi hrapavosti površja: Razredi hrapavosti površja so izpeljani iz mere hrapavosti (Z_0), ki je merilo aerodinamične hrapavosti površja. Ta je opredeljena kot višina, na kateri nevtralni profil vetra pri tleh doseže hitrost 0 m/s (Oke, 2002). Z_0 izračunamo s formulo 2, pri čemer je f_0 koeficient hrapavost (0,1), $\overline{Z_H}$ pa povprečna višina elementov v prostoru (Hammond in sod., 2012). Za izračun razredov hrapavosti površja smo iz nDMP brez upoštevanja celic z vrednostjo 0 m za vsak poligon mreže izračunali $\overline{Z_H}$. Upoštevali smo višine stavb, nizkega, srednje visokega in visokega rastlinstva. Vrednosti Z_0 smo nato pretvorili v razrede hrapavosti površja glede na preglednico 2.

$$Z_0 = f_0\overline{Z_H}$$

(Formula 2)

Preglednica 2: Opredelitev razredov hrapavosti površja.

Z_0	Razredi hrapavosti površja
0,0000–0,0020	1
0,0021–0,0050	2
0,0051–0,0300	3
0,0301–0,1000	4
0,1001–0,2500	5
0,2501–0,5000	6
0,5001–1,0000	7
> 1,0000	8

Vir: Davenport in sod., 2000.

Slika 2: Zemljevidi ustvarjenih slojev vhodnih podatkov za klasifikacijo LPO.

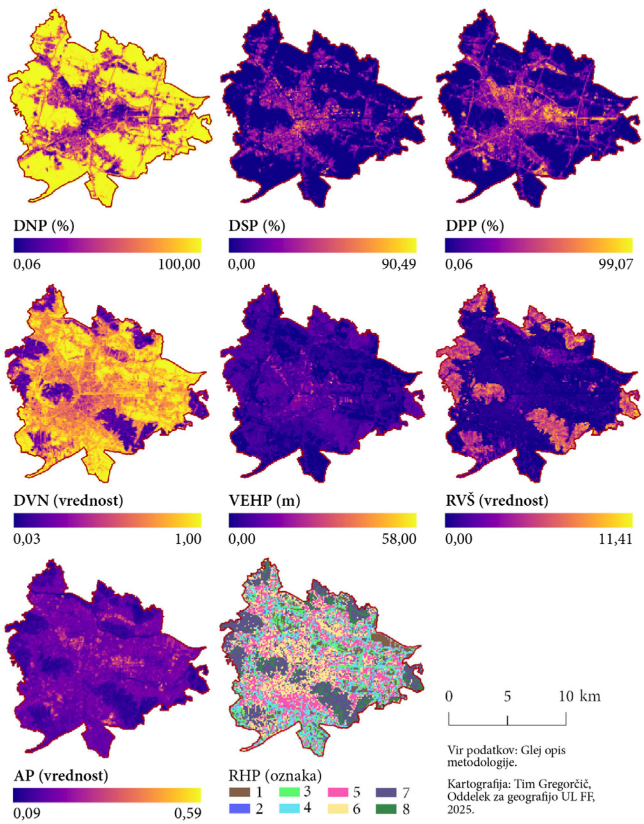

Albedo površja: Sloj albeda površja (razmerje med količino Sončevega sevanja, ki ga površje odbije, in celotno količino prejetega Sončevega sevanja) je bil izračunan na podlagi satelitskih posnetkov Landsat z dne 20. julija 2022 (USGS, 2022). Uporabili smo metodologijo, ki so jo opisali Silva in sod. (2016), Chander in Markham (2003) ter Allen in sod. (2002). Njihov pristop smo nadgradili z izračunom korekcijskega faktorja zračnega tlaka (razlika med modelno in izmerjeno vrednostjo na območju meteorološke postaje Ljubljana Bežigrad), s katerim smo izboljšali rezultat modeliranega zračnega tlaka. Vse ustvarjene pojasnjevalne spremenljivke za klasifikacijo LPO prikazuje slika 2.

2.2 Standardizacija slojev pojasnjevalnih spremenljivk

Pred klasifikacijo LPO je bila potrebna standardizacija slojev pojasnjevalnih spremenljivk, opisanih v poglavju 2.1., glede na kvantitativno opredelitev tipov LPO. Standardizirani sloji so vsebovali vrednosti intervala od 0 do 1, pri čemer je bila vrednost 1 dodeljena celicam, ki pripadajo določenemu LPO, kot je opredeljeno v preglednici 3. Standardizacijo smo izvedli s kombiniranim postopkom pretvorbe s funkcijo *fuzzy* programskega orodja TerrSet. Meja začetka višanja vrednosti in začetka njihovega nižanja je bila določena glede na interval izbrane spremenljivke, ki definira posamezen tip LPO (slika 3, preglednica 3) (Unger in sod., 2014). Ustvarjenih je bilo 136 standardiziranih slojev (8 za vsako LPO). Z uporabo programskega orodja ArcGIS Pro je bilo vseh 8 slojev za vsako LPO združenih v en sloj z orodjem *Fuzzy Overlay*. Uporabili smo Boolovo logiko »in«, s čimer smo minimizirali »trgovanje« vrednosti med sloji (Estacio in sod., 2019).

Slika 3: Shematski prikaz standardizacije slojev pojasnjevalnih spremenljivk.

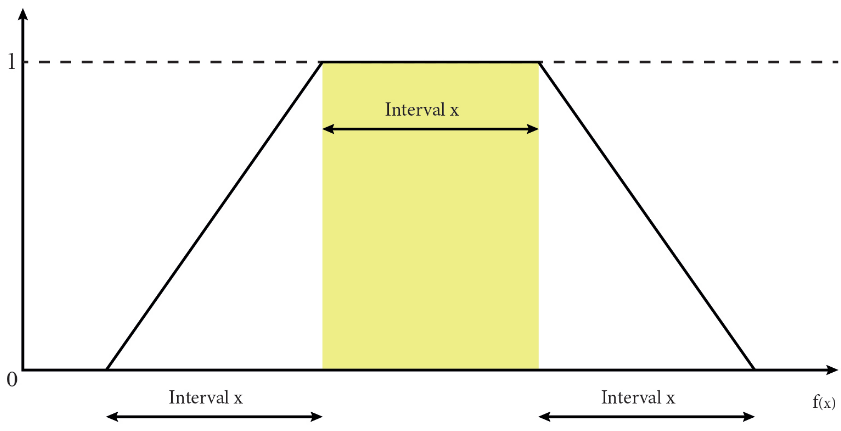

Vir: Unger in sod., 2014

Preglednica 3: Kvantitativna opredelitev lokalnih podnebnih območij glede na pojasnjevalne spremenljivke.

LPO	DVN	RVŠ	DSP	DPP	DNP	VEHP	RHP	AP
LPO 1	0,2–0,4	> 2	40–60	40–60	< 10	> 25	8	0,10–0,20
LPO 2	0,3–0,6	0,75–2	40–70	30–50	< 20	10–25	6–7	0,10–0,20
LPO 3	0,2–0,6	0,75–1,5	40–70	20–50	< 30	3–10	6	0,10–0,20
LPO 4	0,5–0,7	0,75–1,25	20–40	30–40	30–40	> 25	7–8	0,12–0,25
LPO 5	0,5–0,8	0,3–0,75	20–40	30–50	20–40	10–25	5–6	0,12–0,25
LPO 6	0,6–0,9	0,3–0,75	20–40	20–50	30–60	3–10	5–6	0,12–0,25
LPO 7	0,2–0,5	1–2	60–90	< 20	< 30	2–4	4–5	0,15–0,35
LPO 8	>0,7	0,1–0,3	30–50	40–50	< 20	3–10	5	0,12–0,25
LPO 9	> 0,8	0,1–0,25	10–20	< 20	60–80	3–10	5–6	0,12–0,25
LPO 10	0,6–0,9	0,2–0,5	20–30	20–40	40–50	5–15	5–6	0,12–0,20
LPO A	< 0,4	> 1	< 10	< 10	> 90	3–30	8	0,10–0,20
LPO B	0,5–0,8	0,25–0,75	< 10	< 10	> 90	3–15	5–6	0,15–0,25
LPO C	0,7–0,9	0,25–1,0	< 10	< 10	> 90	< 2	4–5	0,15–0,30
LPO D	> 0,9	< 0,1	< 10	< 10	> 90	< 1	3–4	0,15–0,25
LPO E	> 0,9	< 0,1	< 10	> 90	< 10	< 0,25	1–2	0,15–0,30
LPO F	> 0,9	< 0,1	< 10	< 10	> 90	< 0,25	1–2	0,20–0,35
LPO G	> 0,9	< 0,1	< 10	< 10	> 90	–	1	0,02–0,10

Vir: Stewart in Oke, 2012.

2.3 Klasifikacija lokalnih podnebnih območij

Izvedli smo dve klasifikaciji LPO z uporabo dveh različnih metod: CA in WUDAPT. Za klasifikacijo z uporabo metode CA smo uporabili *Python* skript, ki so ga razvili in uporabili Estacio in sod. (2019) v svoji klasifikacijski študiji. Za pojasnjevalne spremenljivke smo uporabili standardizirane sloje, opisane v poglavju 2.2, kodo pa smo zagnali v programskem orodju ArcGIS Pro.

Za klasifikacijo LPO z uporabo metode WUDAPT smo najprej ustvarili učna območja. Prostorsko so bila določena glede na taiste končne standardizirane sloje, ki so bili uporabljeni v primeru klasifikacije z uporabo metode CA. Območja slojev z vrednostjo 0,9 ali več smo upoštevali kot primerna. V primeru LPO 8 smo izjemoma kljub nizkim vrednostim standardiziranega sloja določili učna območja, saj glede na opis ta tip LPO obsega znaten del proučevanega območja (na primer BTC City Ljubljana, nakupovalno središče Rudnik, industrijska cona Šiška itd.). Učna območja so bila nato v formatu KML naložena na spletno platformo WUDAPT, postopek klasifikacije pa je bil izveden z uporabo podatkov Landsat 8, Sentinel 1, Sentinel 2 in drugih virov (Demuzere in sod., 2021). V zadnjem koraku je bila surova klasifikacija generalizirana z uporabo postopka za generalizacijo klasificiranih rastrskih podatkov (Generalization of classified raster imagery—ArcMap | Documentation, b. d.).

2.4 Preverba kakovosti klasifikacij

Identifikacija najustreznejše klasifikacije je temeljila na kombinaciji kvantitativnega ovrednotenja in strokovne presoje. Kvantitativno vrednotenje je bilo izvedeno glede na zmožnost pojasnjevanja prostorskih razlik v pojavnosti prizemnega MTO in TP. Iz podatkov satelitov Landsat 8 in Landsat 9 smo izračunali sloj povprečne temperature površja tako, da smo sledili metodologiji Sobrina in sod. (2004) ter Avdana in Jovanovske (2016). Povprečno TP smo izračunali iz podatkov za 30. junij, 8. julij in 15. julij 2023 (USGS, 2023c, 2023b, 2023a). Sloj poletnega prizemnega MTO smo izračunali iz podatkov raziskave Ogrina in sod. (2022). Za vsak razred obeh klasifikacij smo ustvarili 17,84 naključnih vzorčnih točk na kvadratni kilometer. Na ta način je bilo v razred z največjo površino umeščenih 1000 naključnih vzorčnih točk. S točkami smo nato vzorčili sloja prizemnega MTO in TP. Zaradi nenormalne porazdelitve vrednosti vzorcev sta bila za analizo razlik med LPO uporabljena neparametrični Kruskal-Wallisov test in Dunnov post-hoc test (McKnight in Najab, 2010). Zaradi statističnih omejitev izbranih metod so bila ovrednotena le LPO, kamor je bilo umeščenih vsaj 30 vzorčnih točk.

3 REZULTATI

Rezultat klasifikacije LPO z uporabo metode CA prikazuje slika 4. S to metodo so bili identificirani 4 pretežno pozidani tipi (LPO 2, LPO 5, LPO 6, LPO 9) in 5 pretežno naravnih tipov (LPO A, LPO B, LPO C, LPO E, LPO F). Med njimi smo kvantitativno ovrednotili LPO 2, LPO 5, LPO 6, LPO A, LPO C in LPO F. V primeru analize razlik v pojavnosti prizemnega MTO je bil rezultat Kruskal–Wallisovega testa statistično značilen ($p < 0,05$). S tem smo zavrnili ničelno hipotezo (H_0), ki pravi, da so vse skupine podmnožice iste populacije, in ugotovili, da obstaja dokaz za potrditev alternativne hipoteze (Ha), ki pravi, da vse skupine niso podmnožice iste populacije (preglednica 4). Rezultati Dunnovega post-hoc testa so pokazali, da so mediane statistično različne v vseh primerih parov LPO ($p < 0,05$), razen med LPO 2 in LPO 5 (preglednica 5). Grafikoni kvartilov na sliki 5 prikazujejo porazdelitev vrednosti prizemnega MTO.

Slika 4: Klasifikacija LPO z uporabo metode CA.

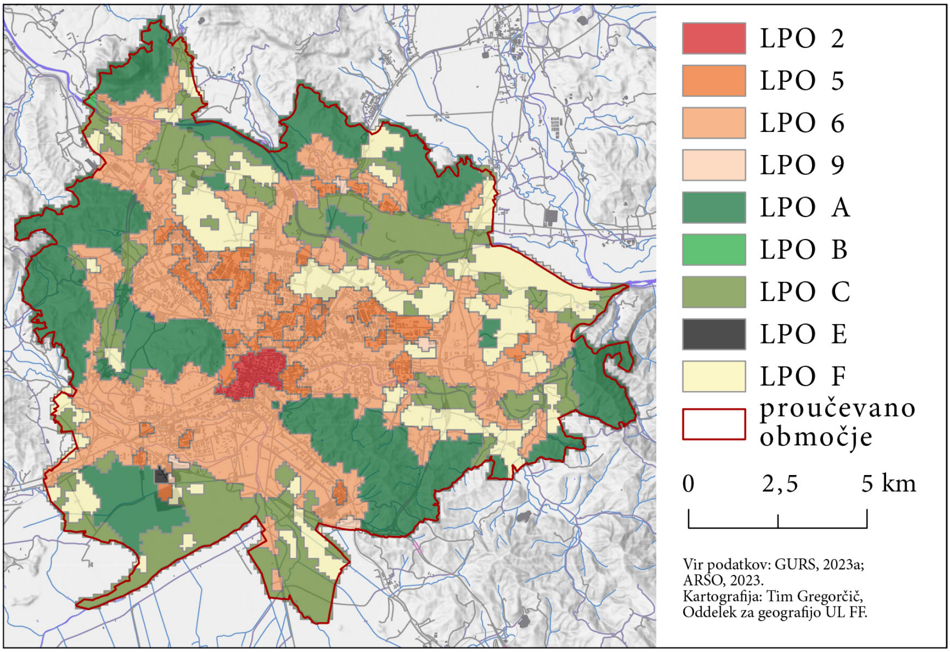

Preglednica 4: Kruskal-Wallisov test razlik vrednosti prizemnega MTO med LPO metode CA.

Kruskal-Wallisov test vsote rangov		
Kruskal-Wallisov hi kvadrat	Df	p vrednost
1485,5	5	< 0,05

Preglednica 5: Dunnov post-hoc test razlik vrednosti prizemnega MTO med pari LPO metode CA.

Dunnov post-hoc test (Bonferroni)							
		LPO 2	LPO 5	LPO 6	LPO A	LPO C
LPO 5	z-vrednost testa	2,02				
	prilag. p-vrednost	0,33				
LPO 6	z-vrednost testa	5,60	7,56			
	prilag. p-vrednost	<0,05	<0,05			

Dunnov post-hoc test (Bonferroni)						
		LPO 2	LPO 5	LPO 6	LPO A	LPO C
LPO A	z-vrednost testa	9,74	16,45	16,27		
	prilag. p-vrednost	<0,05	<0,05	<0,05		
LPO C	z-vrednost testa	14,33	25,61	30,71	15,62	
	prilag. p-vrednost	<0,05	<0,05	<0,05	<0,05	
LPO F	z-vrednost testa	12,25	20,77	21,89	8,32	-5,69
	prilag. p-vrednost	<0,05	<0,05	<0,05	<0,05	<0,05

Slika 5: Porazdelitev vrednosti prizemnega MTO glede na tip LPO metode CA.

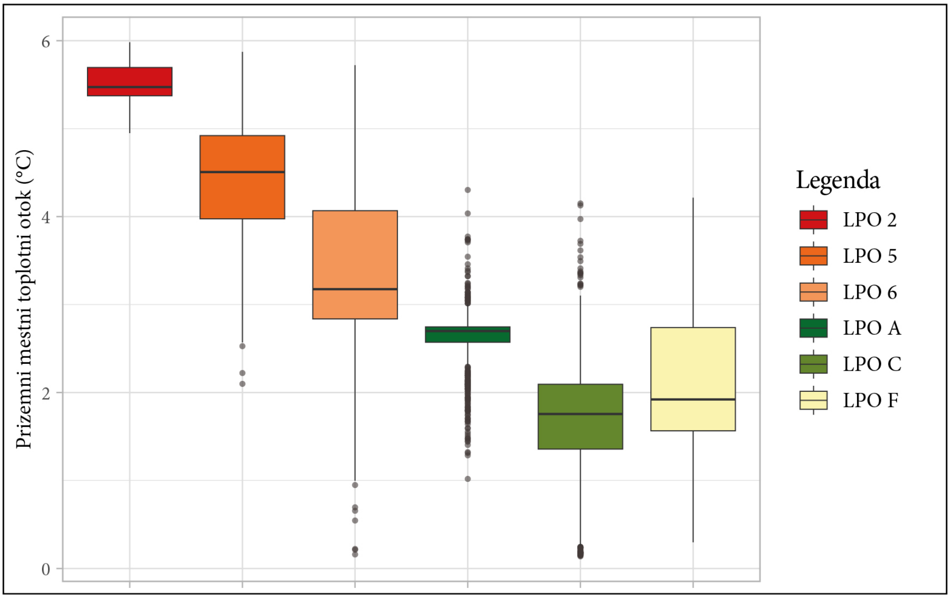

V primeru analize razlik v vrednostih TP med LPO smo s Kruskal-Wallisovim testom ponovno ovrgli H_0 ($p < 0,05$) (preglednica 6). Z Dunnovim post-hoc testom smo ugotovili enake odnose med pari LPO, kot smo jih opazili v primeru prizemnega MTO (preglednica 7). LPO 2 in LPO 5 je bil edini par, za katerega ni bila ugotovljena statistično značilna razlika. Slika 6 prikazuje porazdelitev vrednosti TP s pomočjo grafikonov kvartilov.

Preglednica 6: Kruskal-Wallisov test razlik vrednosti TP med LPO metode CA.

Kruskal-Wallisov test vsote rangov		
Kruskal-Wallisov hi kvadrat	Df	p vrednost
2200,4	5	< 0,05

Preglednica 7: Dunnov post hoc test razlik vrednosti TP med pari LPO metode CA.

Dunnov post-hoc test (Bonferroni)						
		LPO 2	LPO 5	LPO 6	LPO A	LPO C
LPO 5	z-vrednost testa	1,18				
	prilag. p-vrednost	1,00				
LPO 6	z-vrednost testa	3,64	5,23			
	prilag. p-vrednost	<0,05	<0,05			
LPO A	z-vrednost testa	14,27	28,32	42,29		
	prilag. p-vrednost	<0,05	<0,05	<0,05		
LPO C	z-vrednost testa	9,93	18,30	22,41	-14,44	
	prilag. p-vrednost	<0,05	<0,05	<0,05	<0,05	
LPO F	z-vrednost testa	7,79	13,46	13,76	-19,78	-6,02
	prilag. p-vrednost	<0,05	<0,05	<0,05	<0,05	<0,05

Rezultat klasifikacije LPO z metodo WUDAPT je prikazan na sliki 7. S to metodo smo določili 4 pretežno pozidane tipe (LPO 2, LPO 5, LPO 6, LPO 8) in 5 pretežno naravnih tipov (LPO A, LPO C, LPO D, LPO F, LPO G). Za razliko od CA so del rezultatov metode WUDAPT različne metrike za oceno uspešnosti klasifikacije glede na njeno ujemanje z učnimi vzorci (slika 8). Splošna natančnost rezultata je dobra, saj je bilo pravilno razvrščenih 76 % učnih celic (*SN = 0,76*). Skupna natančnost pretežno pozidanih LPO (SNu) je znašala 0,70. Glede na primerjavo med pretežno pozidanimi in pretežno naravnimi LPO brez upoštevanja razlik znotraj skupin je bilo pravilno klasificiranih 99 % učnih celic (SNun). Skupna ponderirana natančnost (SNp), ki upošteva (ne)podobnost med tipi LPO in bolj kaznuje zamenjavo med nepodobnimi tipi kot zamenjavo med podobnimi tipi, je znašala 0,95 (Demuzere in sod., 2021). Točnost posameznega tipa, ovrednotena z metriko F1, je bila v vseh primerih, razen v primeru LPO 5, višja od 0,75. S tem lahko rezultate v splošnem ocenimo kot dobre (Chicco in Jurman, 2020).

Slika 6: Porazdelitev vrednosti TP glede na tip LPO metode CA.

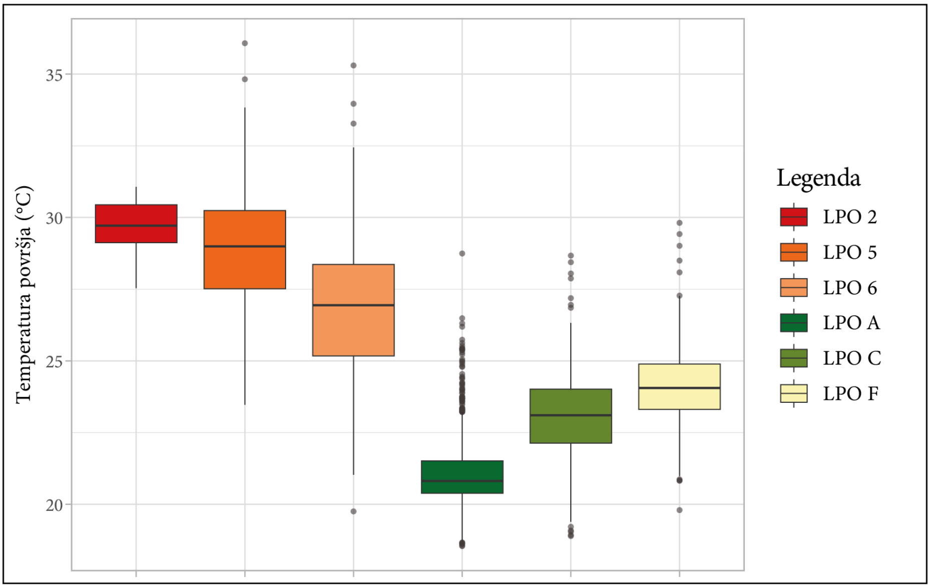

Slika 7: Klasifikacija LPO z uporabo metode WUDAPT.

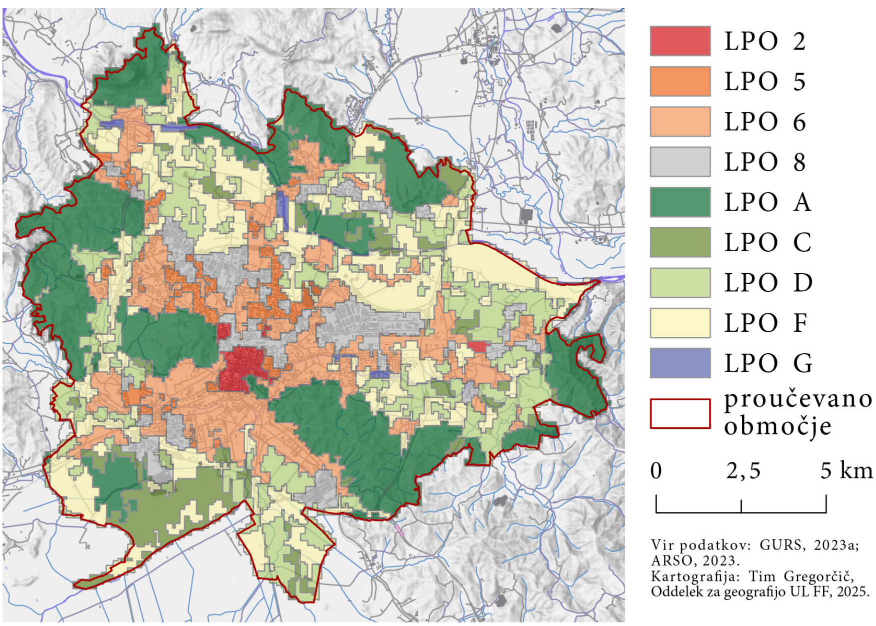

Slika 8: Ocena natančnosti rezultatov klasifikacije z uporabo metode WUDAPT.

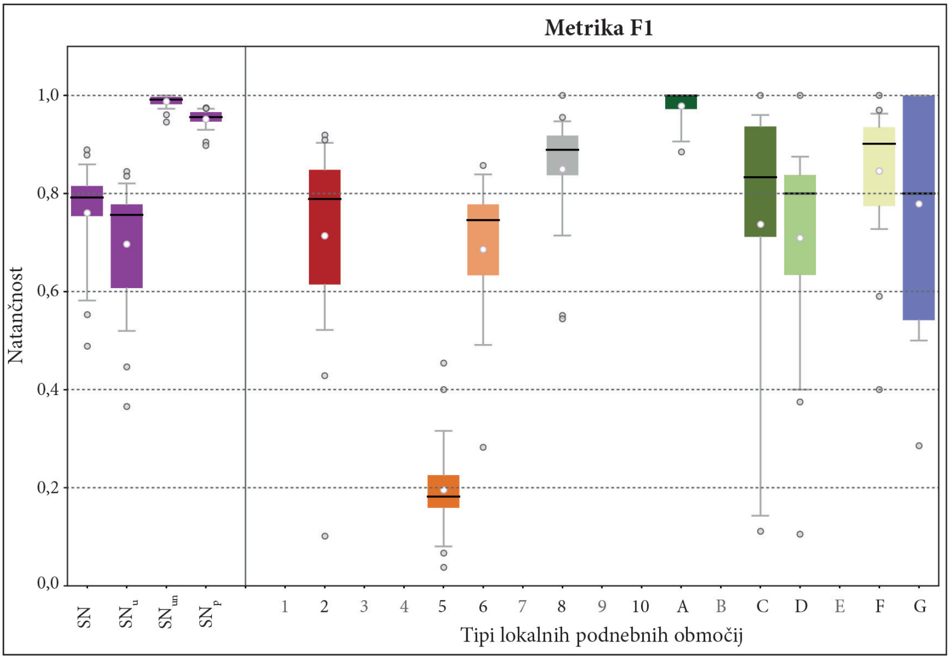

V sklopu vrednotenja klasifikacije metode WUDAPT glede na sloja TP in prizemnega MTO smo upoštevali LPO 2, LPO 5, LPO 6, LPO 8, LPO A, LPO C, LPO D in LPO F. V primeru analize razlik v pojavnosti prizemnega MTO je bil rezultat Kruskal–Wallisovega testa statistično značilen ($p < 0,05$). S tem smo ponovno zavrnili H_0 in potrdili H_a (preglednica 8). Rezultati Dunnovega post-hoc testa so pokazali, da so mediane statistično različne v vseh primerih parov LPO ($p < 0,05$), razen med LPO 2 in LPO 5, LPO 2 in LPO 8, LPO 5 in LPO 8 ter LPO C in LPO D (preglednica 9). Grafikoni kvartilov na sliki 9 prikazujejo porazdelitev vrednosti prizemnega MTO.

Preglednica 8: Kruskal-Wallisov test razlik vrednosti prizemnega MTO med LPO metode WUDAPT.

Kruskal-Wallisov test vsote rangov		
Kruskal-Wallisov hi kvadrat	Df	p vrednost
1440,1	7	< 0,05

Preglednica 9: Dunnov post-hoc test razlik vrednosti prizemnega MTO med pari LPO metode WUDAPT.

Dunnov post-hoc preizkus (Bonferroni)								
		LPO 2	LPO 5	LPO 6	LPO 8	LPO A	LPO C	LPO D
LPO 5	z-vrednost testa	1,79						
	prilag. p-vrednost	1,00						
LPO 6	z-vrednost testa	3,91	2,95					
	prilag. p-vrednost	<0,05	0,04					
LPO 8	z-vrednost testa	2,50	0,91	−2,94				
	prilag. p-vrednost	0,18	1,00	0,046				
LPO A	z-vrednost testa	9,38	11,66	16,53	15,72			
	prilag. p-vrednost	<0,05	<0,05	<0,05	<0,05			
LPO C	z-vrednost testa	12,95	16,12	19,92	19,72	9,33		
	prilag. p-vrednost	<0,05	<0,05	<0,05	<0,05	<0,05		
LPO D	z-vrednost testa	13,14	17,35	25,63	23,30	11,63	-1,02	
	prilag. p-vrednost	<0,05	<0,05	<0,05	<0,05	<0,05	1,00	
LPO F	z-vrednost testa	11,66	15,16	22,44	20,50	7,39	-4,27	-4,44
	prilag. p-vrednost	<0,05	<0,05	<0,05	<0,05	<0,05	<0,05	<0,05

Slika 9: Porazdelitev vrednosti prizemnega MTO glede na tip LPO metode WUDAPT.

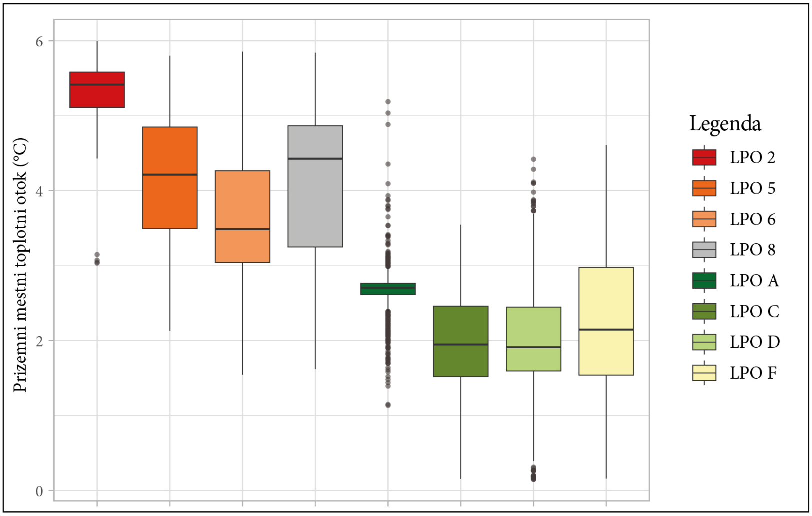

Po analizi razlik v vrednostih TP med LPO metode WUDAPT smo s Kruskal-Wallisovim testom ponovno ovrgli H_0 ($p < 0{,}05$) (preglednica 10). Na podlagi Dunnovega post-hoc testa lahko zavrnemo H_0 v vseh primerih, razen pri LPO 2 in LPO 5, LPO 2 in LPO 6, LPO 2 in LPO 8, LPO 5 in LPO 6, LPO 5 in LPO 8 ter LPO D in LPO F (preglednica 11). To pomeni, da se v vseh parih LPO, razen v zgoraj omenjenih, mediane TP med seboj pomembno razlikujejo. Slika 10 prikazuje porazdelitev vrednosti TP s pomočjo grafikonov kvartilov.

Preglednica 10: Kruskal-Wallisov test razlik vrednosti prizemnega MTO med LPO metode WUDAPT.

Kruskal-Wallisov test vsote rangov		
Kruskal-Wallisov hi kvadrat	Df	p vrednost
2273,4	7	< 0,05

Preglednica 11: Dunnov post hoc test razlik vrednosti prizemnega MTO med pari LPO metode WUDAPT.

Dunnov post-hoc test (Bonferroni)								
		LPO 2	LPO 5	LPO 6	LPO 8	LPO A	LPO C	LPO D
LPO 5	z-vrednost testa	1,95						
	prilag. p-vrednost	0,72						
LPO 6	z-vrednost testa	2,71	0,78					
	prilag. p-vrednost	0,10	1,00					
LPO 8	z-vrednost testa	0,97	-1,72	-3,79				
	prilag. p-vrednost	1,00	1,00	<0,05				
LPO A	z-vrednost testa	15,11	20,51	38,18	32,98			
	prilag. p-vrednost	<0,05	<0,05	<0,05	<0,05			
LPO C	z-vrednost testa	12,10	14,65	20,72	21,06	-4,78		
	prilag. p-vrednost	<0,05	<0,05	<0,05	<0,05	<0,05		
LPO D	z-vrednost testa	8,51	9,85	16,27	16,65	-19,83	-8,68	
	prilag. p-vrednost	<0,05	<0,05	<0,05	<0,05	<0,05	<0,05	
LPO F	z-vrednost testa	8,36	9,69	16,48	16,70	-21,60	-9,29	-0,55
	prilag. p-vrednost	<0,05	<0,05	<0,05	<0,05	<0,05	<0,05	1,00

Slika 10: Porazdelitev vrednosti prizemnega MTO glede na tip LPO metode WUDAPT.

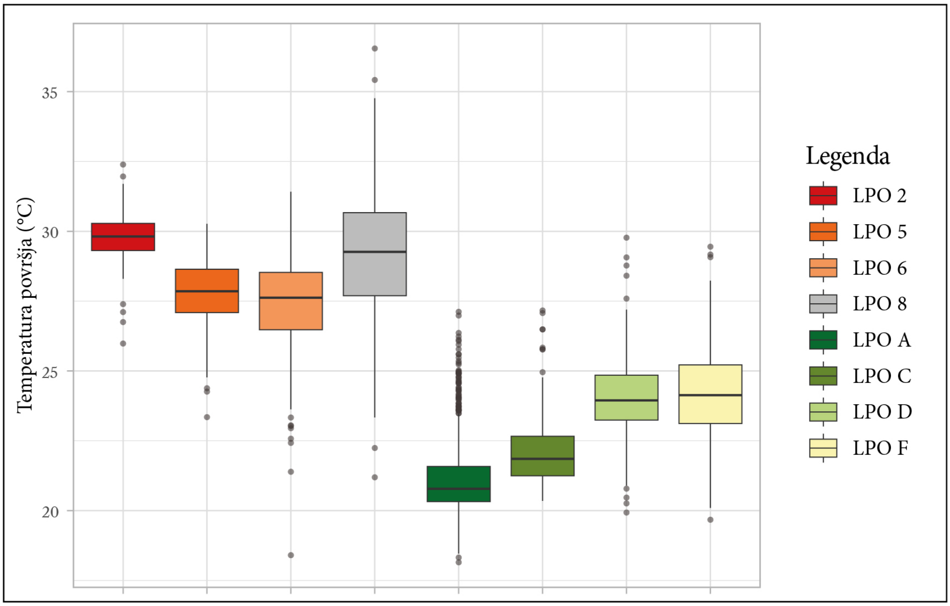

4 RAZPRAVA

V raziskavi smo izvedli klasifikacijo LPO Ljubljane z uporabo metod CA in WUDAPT. Glede na naše vedenje gre za prvi poglobljeni poizkus klasifikacije LPO Ljubljane, ki sledi metodologiji Stewarta in Oka (2012). Kakovost rezultatov smo ocenili na podlagi razlik v vrednostih prizemnega MTO in TP med LPO. Pomembno je zavedanje, da smo z obema kazalcema uspešnost klasifikacije ovrednotili le glede na razmere v času povprečnega poletnega radiacijskega tipa vremena.

Vizualna primerjava kart LPO kaže, da sta si rezultata kljub uporabi fundamentalno različnih klasifikacijskih metod zelo podobna (sliki 4 in 7). To potrjuje zanesljivost rezultatov glede na neodvisne spremenljivke, ki definirajo LPO. Glavna razlika med rezultatoma za pretežno pozidana LPO (LPO 1–LPO 10) je, da so bili z metodo WUDAPT identificirani 4 tipi LPO, ki zavzemajo nezanemarljiv delež mestnega območja (LPO 2: kompaktna srednje visoka gradnja, LPO 5: odprta srednje visoka gradnja, LPO 6: odprta nizka gradnja in LPO 8: velikopovršinska nizka gradnja), z metodo CA pa 3 nezanemarljivi tipi (LPO 2, LPO 5 in LPO 6). Območja, ki so z metodo WUDAPT identificirana kot LPO 8, so v primeru klasifikacije CA vključena v LPO 6. Nezmožnost identifikacije LPO 8 je v skladu s študijo klasifikacije LPO filipinskega mesta Quezon, ki so jo izvedli avtorji metode, uporabljene v naši raziskavi (Estacio in sod., 2019). Na pogosta razhajanja v številu identificiranih LPO istega območja zaradi uporabe različnih klasifikacijskih metod so opozorile že študije za Dunaj (Hammerberg in sod., 2018) in Brno (Geletič in Lehnert, 2016). V primeru te raziskave menimo, da je glavni razlog za razhajanja nedostopnost GIS sloja antropogenega prispevka toplote, saj je ta spremenljivka ključna za razlikovanje LPO 8 in LPO 10 od drugih pretežno pozidanih tipov LPO (Stewart in Oke, 2012).

Kruskal-Wallisova testa sta pokazala, da se mediane LPO obeh klasifikacijskih metod glede na prizemni MTO statistično značilno razlikujejo. Tudi glede na rezultate Dunnovih post-hoc testov se mediane prizemnega MTO večine parov pretežno pozidanih LPO statistično značilno razlikujejo. Pri obeh klasifikacijah je izjema razlika med LPO 2 in LPO 5. Razlog za to bi lahko bila morfologija Ljubljane, saj v mestu ni obsežnih blokovskih sosesk, ki so običajne v mnogih drugih večjih evropskih mestih. To lahko ovira razvoj specifičnega temperaturnega režima. Kljub statistično neznačilnim razlikam so na slikah 5 in 9 jasno vidne diskrepance med kvartilnimi razmiki, kar kaže na opazne razlike v intenzivnosti med obema tipoma LPO. V primeru metode WUDAPT razlike niso bile statistično značilne tudi v primerih LPO 2 in LPO 8 ter LPO 5 in LPO 8. Glede na dinamiko prizemnega MTO v Ljubljani, kjer je pojav najintenzivnejši v mestnem središču in na industrijskih ali trgovskih središčih (Ogrin in sod., 2022, 2023), bistvenih razlik med LPO 2 in LPO 8 ni mogoče upravičeno pričakovati.

Med vrednotenjem rezultatov obeh klasifikacij smo zaznali metodološko omejitev izdelave sloja prizemnega MTO Ogrina in sodelavcev (2022). Avtorji so sloj ustvarili s prostorsko interpolacijo točkovnih meritev, za kar so uporabili metodo navadnega kriginga. Zaradi manjše gostote merilnih mest na gozdnih območjih in njihove specifične prostorske razporeditve so gozdnim območjem v primerjavi s travniki pripisali višje vrednosti intenzivnosti pojava. To na splošno ni v skladu z značilnimi temperaturnimi razmerji med gozdnimi in travnatimi površinami (Shen in sod., 2017). Posledično ugotovitvam o statistično značilnih razlikah prizemnega MTO med LPO zaradi omejitve vhodnih podatkov ne moremo v celoti zaupati. Metodološko bi bila najprimernejša uporaba točkovnih podatkov meritev Ogrina in sod. (2023), a zaradi premajhnega števila točk ne bi zadostili pogojem uporabljenih statističnih metod.

Kruskal-Wallisova testa sta pokazala, da se mediane LPO, pridobljene z obema metodama klasifikacije, statistično značilno razlikujejo tudi glede na TP. Pri uporabi metode CA se le mediani LPO 2 in LPO 5 nista razlikovali statistično značilno. V primeru klasifikacije z uporabo metode WUDAPT so bile statistično značilne razlike med pretežno pozidanimi tipi LPO opažene le med LPO 6 in LPO 8. To kaže, da so s statističnega vidika prostorske razlike TP med LPO v poznih dopoldanskih urah in ob prisotnosti radiacijskega tipa poletnega vremena majhne.

Z metodo WUDAPT smo ustvarili zanesljiv rezultat z vidika razlikovanja med pretežno pozidanimi in pretežno naravnimi LPO (slika 8). Metrika F1 je za LPO 5 znašala manj kot 0,2, kar potrjuje hipotezo, da je prepoznavanje tega tipa zahtevno zaradi specifičnih morfoloških značilnosti mesta. Splošna natančnost rezultata (*SN* = 0,76) je primerljiva z natančnostjo klasifikacij bližnjih mest (npr. Zagreb 0,43–0,81; Novi Sad 0,81; Dunaj 0,59; Milano 0,35–0,72) (Demuzere in sod., 2021). Čeprav so rezultati primerljivi, nakazujejo tudi, da bi bile v prihodnosti smiselne nadaljnje izboljšave klasifikacije. Ob primerjavi klasifikacij Ljubljane, Zagreba in Novega Sada ugotavljamo, da vsa tri mesta pretežno sestavljajo LPO 2, LPO 5 in LPO 6. Glavna razlika med slovensko prestolnico in drugima dvema mestoma je, da na območju Ljubljane ni LPO 3 (kompaktna nizka gradnja) (Demuzere in sod., 2021). Kot alternativo metodi WUDAPT so Milošević in sod. (2022) za območje Novega Sada uporabili tudi metodologijo Lelovicsa in sod. (2014). Tudi s to klasifikacijo so avtorji identificirali vzorce, podobne klasifikaciji LPO Ljubljane, vendar so dodatno locirali LPO 10, ki je odsotno v obeh naših različicah.

Ker je bila študija osredotočena predvsem na pretežno pozidana LPO z večjo gostoto prebivalstva in izrazitejšo prisotnostjo človekovih dejavnosti, razlike med pretežno naravnimi LPO niso bile ovrednotene z enako mero podrobnosti. Eden od razlogov za to je tudi, da so gozdne površine in vodna telesa edina tipa rabe tal, ki skozi čas z vidika prostorske pojavnosti ostajata relativno stabilna, medtem ko se značilnosti rabe kmetijskih zemljišč letno spreminjajo.

Na podlagi analiz je bilo treba izbrati ustreznejšo izmed obeh klasifikacij. Čeprav smo z uporabo obeh metod ustvarili podobne rezultate, so bila zgolj z uporabo metode WUDAPT nakupovalna in industrijska središča umeščena v LPO 8 (velikopovršinska nizka gradnja). Znano je, da so ti deli mesta med območji z najvišjimi TP (Komac in sod., 2016), temperaturami zraka in intenzivnostjo prizemnega MTO (Ogrin in sod., 2022, 2023). Posledično menimo, da je klasifikacija metode WUAPT bolj reprezentativna in uporabna kljub temu, da smo s statističnimi metodami potrdili manj razlik v TP in prizemnem MTO med LPO v primerjavi z rezultatom metode CA.

S to študijo smo razvili mikroklimatološko klasifikacijo Ljubljane, ki omogoča standardizirane meteorološke in podnebne raziskave v mestih (Wang in sod., 2024). Klasifikacija je lahko osnova za nadaljnje raziskave MTO in razvoj novih raziskovalnih področij, kot sta zunanja toplotna obremenitev ljudi (Cao in sod., 2022; Lam in sod., 2023) in značilnosti vlažnosti zraka v mestu (Dunjić in sod., 2021; Yang in sod., 2020). Rezultat je lahko uporaben tudi kot vhodni podatek za regionalne podnebne modele (Ribeiro in sod., 2021; Wang in sod., 2024), študije porabe energije v stavbah (Kotharkar in sod., 2022; Tian in sod., 2024) ter urbanistično oblikovanje in načrtovanje (He in sod., 2024; Wang in sod., 2024).

Kljub multidisciplinarni aplikativnosti klasifikacije se je treba zavedati, da gre pri njej izključno za morfološko delitev mesta in da ne izhaja iz kakršnihkoli meteoroloških meritev, kljub temu da v svojem imenovanju vključuje termin »podnebje«. LPO *a priori* torej ne opredeljujejo tipov mestnega podnebja, temveč zagotavljajo dobro podlago za podnebne študije na omenjenih raziskovalnih področjih. Po trditvah Stewarta in Oka (2012) je za vsako LPO značilen specifičen toplotni režim, ki je najbolj izrazit nad suhimi površinami v mirnih in jasnih nočeh ter na območjih z enostavno topografijo. Čeprav so razlike v temperaturi zraka in drugih meteoroloških spremenljivkah med LPO pogosto opazne, na podlagi te klasifikacije ni mogoče izpeljati splošnih značilnosti mestnega podnebja (Huang in sod., 2023).

Čeprav predstavljena klasifikacija LPO Ljubljane dosledno sledi metodologiji Stewarta in Oka (2012) in je bila kvantitativno in kvalitativno ovrednotena, je še veliko prostora za njeno izboljšavo in nadaljnje analize. Našo študijo je omejevalo pomanjkanje podatkov za dve ključni prostorski spremenljivki: toplotna admitanca in antropogeni prispevek toplote. Nedostopnost nekaterih pojasnjevalnih spremenljivk je pogosta omejitev v podobnih študijah (Lehnert in sod., 2021), zato se postavlja vprašanje, ali bi bilo smiselno metodološki okvir na novo opredeliti in optimizirati, da bi omogočili večjo dostopnost do zahtevanih podatkov. Kljub uporabi najsodobnejših razpoložljivih zbirk podatkov za razvoj prostorskih slojev pojasnjevalnih spremenljivk so bili nekateri viri, na primer lidarski podatki, stari skoraj desetletje. Posledično rezultati razširjenosti LPO v celoti ne odražajo trenutnega stanja, zato bi jih bilo v prihodnosti koristno posodobiti. Ker pretežno naravni tipi LPO zaradi predhodno omenjenih omejitev niso bili v središču pozornosti te študije, je treba v prihodnjih raziskavah večji poudarek nameniti tudi tem delom mesta. Poleg tega je treba preizkusiti še druge napredne klasifikacijske metode, kot so nevronske mreže in naključni gozdovi (Cui in sod., 2022). Dodati je treba še, da je bila klasifikacija kvantitativno ovrednotena izključno za čas „idealnih“ vremenskih razmer, ki so ugodne za nastanek poletnega MTO, zato je treba njeno relevantnost v drugih vremenskih razmerah in letnih časih še naknadno proučiti.

5 ZAKLJUČEK

Namen raziskave je bil klasificirati LPO Ljubljane glede na opredelitev Stewarta in Oka (2012), da bi omogočili standardizirane raziskave s področja mestnega vremena, podnebja in drugih znanstvenih disciplin. Ustvarili smo prostorske podatke, potrebne za klasifikacijo LPO (C1), klasificirali LPO Ljubljane z uporabo metod CA in WUDAPT (C2 in C3) ter ovrednotili rezultate obeh metod na podlagi njune sposobnosti pojasnjevanja prostorske spremenljivosti TP in prizemnega MTO ter na podlagi strokovne presoje (C4). Klasifikacija, ustvarjena z metodo WUDAPT, je bila prepoznana kot primernejša in uporabna za prihodnje raziskave, saj lahko z njo v dobršni meri pojasnimo kvantitativne razlike intenzivnosti poletnega prizemnega MTO in TP, poleg tega smo z njo kot ločen tip identificirali tudi velikopovršinsko nizko gradnjo (LPO 8), kamor uvrščamo industrijske cone in večja nakupovalna središča. Temu ni bilo tako v primeru metode CA. Z metodo WUDAPT smo identificirali štiri pretežno pozidane in pet pretežno naravnih tipov LPO.

Zahvala

Avtorji se iskreno zahvaljujemo dr. Estaciu in njegovim sodelavcem za prijazno posredovanje orodja CA, ki je bilo temeljni pogoj za to študijo.

Literatura in viri

Allen, R. G., Tasumi, M. in Trezza, R. (2002). SEBAL (Surface Energy Balance Algorithms for Land)-Advanced training and user's manual-Idaho implementation, Version 1.0. https://posmet.ufv.br/wp-content/uploads/2017/04/MET-479-Waters-et-al-SEBAL.pdf

ARSO [Agencija Republike Slovenije za okolje]. (2011). *Podatki zračnega laserskega skeniranja* [Prostorski podatki]. https://gis.arso.gov.si/evode/profile.aspx?id=atlas_voda_Lidar%40Arso&initialExtent=402591.76%2C39904.09%2C2.64583

Assaf, G. in Assaad, R. H. (2024). Modeling the impact of land use/land cover (LULC) factors on diurnal and nocturnal Urban Heat Island (UHI) intensities using spatial regression models. *Urban Climate*, *55*, 101971. https://doi.org/10.1016/j.uclim.2024.101971

Avdan, U. in Jovanovska, G. (2016). Algorithm for land surface temperature using LANDSAT 8 Satellite Data. *Journal of Sensors*, *2016*, 1480307. https://doi.org/10.1155/2016/1480307

Cao, Q., Huang, H., Hong, Y., Huang, X., Wang, S., Wang, L. in Wang, L. (2022). Modeling intra-urban differences in thermal environments and heat stress based on local climate zones in central Wuhan. *Building and Environment*, *225*, 109625. https://doi.org/10.1016/j.buildenv.2022.109625

Chander, G. in Markham, B. (2003). Revised Landsat-5 TM radiometric calibration procedures and postcalibration dynamic ranges. *IEEE Transactions on Geoscience and Remote Sensing*, *41*(11), 2674–2677. https://doi.org/10.1109/TGRS.2003.818464

Chicco, D. in Jurman, G. (2020). The advantages of the Matthews correlation coefficient (MCC) over F1 score and accuracy in binary classification evaluation. *BMC Genomics*, *21*(1), 6. https://doi.org/10.1186/s12864-019-6413-7

Chien-Ta, C., Chia-Tse, H., Jyh-Dong, L. in Po-Hsun, S. (2015). Application of a decision tree method with a spatiotemporal object database for pavement maintenance and management. *Journal of Marine Science and Technology*, *23*(3), 302–307. https://doi.org/10.6119/JMST-014-0327-5

Ciglič, R. in Komac, B. (2014). Urban heat Island Atlas: A web tool for the determination and mitigation of urban heat Island effects. *Geographia Polonica*, *87*(4), 587–591.

Cui, S., Wang, X., Yang, X., Hu, L., Jiang, Z. in Feng, Z. (2022). Mapping local climate zones in the urban environment: The optimal combination of data source and classifier. *Sensors*, *22*(17), 6407. https://doi.org/10.3390/s22176407

Davenport, A. G., Grimmond, S., Oke, T. in Wieringa, J. (2000). Estimating the roughness of cities and sheltered country. *15th conference on probability and statistics in the atmospheric sciences/12th conference on applied climatology, Ashville, NC, American Meteorological Society*, 96–99.

Demuzere, M., Kittner, J. in Bechtel, B. (2021). LCZ generator: A web application to create local climate zone maps. *Frontiers in Environmental Science*, *9*, 637455. https://doi.org/10.3389/fenvs.2021.637455

Demuzere, M., Kittner, J., Martilli, A., Mills, G., Moede, C., Stewart, I. D., van Vliet, J. in Bechtel, B. (2022). A global map of local climate zones to support earth system modelling and urban-scale environmental science. *Earth System Science Data*, *14*(8), 3835–3873. https://doi.org/10.5194/essd-14-3835-2022

Dunjić, J., Milošević, D., Kojić, M., Savić, S., Lužanin, Z., Šećerov, I. in Arsenović, D. (2021). Air humidity characteristics in “local climate zones” of Novi Sad (Serbia) based on long-term data. *ISPRS International Journal of Geo-Information*, *10*(12), 810. https://doi.org/10.3390/ijgi10120810

Estacio, I., Babaan, J., Pecson, N. J., Blanco, A. C., Escoto, J. E. in Alcantara, C. K. (2019). GIS-based mapping of local climate zones using fuzzy logic and cellular automata. *International Archives of the Photogrammetry, Remote Sensing and Spatial Information Sciences*, *XLII-4/W19*, 199–206. https://doi.org/10.5194/isprs-archives-XLII-4-W19-199-2019

Geletič, J. in Lehnert, M. (2016). GIS-based delineation of local climate zones: the case of medium-sized central European cities. *Moravian Geographical Reports*, *24*(3), 2–12. https://doi.org/doi:10.1515/mgr-2016-0012

Generalization of classified raster imagery—ArcMap | Documentation. (b. d.). https://desktop.arcgis.com/en/arcmap/latest/tools/spatial-analyst-toolbox/generalization-of-classified-raster-imagery.htm

Goward, S. N., Markham, B., Dye, D. G., Dulaney, W. in Yang, J. (1991). Normalized difference vegetation index measurements from the advanced very high resolution radiometer. *Remote Sensing of Environment*, *35*(2), 257–277. https://doi.org/10.1016/0034-4257(91)90017-Z

GURS [Geodetska uprava Republike Slovenije]. (2015). *Digitalni ortofoto* [Prostorski podatki]. https://ipi.eprostor.gov.si/jv/?map=jgp

GURS. (2023a). *Kataster nepremičnin* [Prostorski podatki]. https://ipi.eprostor.gov.si/jgp/data

GURS. (2023b). *Register prostorskih enot* [Prostorski podatki]. https://ipi.eprostor.gov.si/jgp/data

Hammerberg, K., Brousse, O., Martilli, A. in Mahdavi, A. (2018). Implications of employing detailed urban canopy parameters for mesoscale climate modelling: a comparison between WUDAPT and GIS databases over Vienna, Austria. *International Journal of Climatology*, *38*(S1), e1241–e1257. https://doi.org/10.1002/joc.5447

Hammond, D. S., Chapman, L. in Thornes, J. E. (2012). Roughness length estimation along road transects using airborne LIDAR data. *Meteorological Applications*, *19*(4), 420–426. https://doi.org/10.1002/met.273

He, B. J., Fu, X., Zhao, Z., Chen, P., Sharifi, A. in Li, H. (2024). Capability of LCZ scheme to differentiate urban thermal environments in five megacities of China: implications for integrating LCZ system into heat-resilient planning and design. *IEEE Journal of Selected Topics in Applied Earth Observations and Remote Sensing*, *17*, 18800–18817. https://doi.org/10.1109/JSTARS.2024.3469241

Hu, M., Zhang, K., Nguyen, Q. in Tasdizen, T. (2023). The effects of passive design on indoor thermal comfort and energy savings for residential buildings in hot climates: A systematic review. *Urban Climate*, *49*, 101466. https://doi.org/10.1016/j.uclim.2023.101466

Huang, F., Jiang, S., Zhan, W., Bechtel, B., Liu, Z., Demuzere, M., Huang, Y., Xu, Y., Ma, L., Xia, W., Quan, J., Jiang, L., Lai, J., Wang, C., Kong, F., Du, H., Miao, S., … Chen, J. (2023). Mapping local climate zones for cities: A large review. *Remote Sensing of Environment*, *292*, 113573. https://doi.org/10.1016/j.rse.2023.113573

Jernej, S. (2000). *Analiza klime Ljubljane*. Inštitut za geografijo Karl-Franzens Univerze.

Kim, M., Jeong, D. in Kim, Y. (2021). Local climate zone classification using a multiscale, multi-level attention network. *ISPRS Journal of Photogrammetry and Remote Sensing*, *181*, 345–366. https://doi.org/10.1016/j.isprsjprs.2021.09.015

Komac, B., Ciglič, R., Loose, A., Pavšek, M., Čermelj, S., Oštir, K., Kokalj, Ž. in Topole, M. (2016). Urban heat island in the Ljubljana city. V F. Musco (ur.), *Counteracting urban heat island effects in a global climate change scenario* (str. 323–344). Springer International Publishing.

Kotharkar, R., Ghosh, A., Kapoor, S. in Reddy, D. G. K. (2022). Approach to local climate zone based energy consumption assessment in an Indian city. *Energy and Buildings*, *259*, 111835. https://doi.org/10.1016/j.enbuild.2022.111835

Lam, C. K. C., Shooshtarian, S. in Kenawy, I. (2023). Assessment of urban physical features on summer thermal perceptions using the local climate zone classification. *Building and Environment*, *236*, 110265. https://doi.org/10.1016/j.buildenv.2023.110265

Lehnert, M., Geletič, J., Husák, J. in Vysoudil, M. (2015). Urban field classification by "local climate zones" in a medium-sized Central European city: the case of Olomouc (Czech Republic). *Theoretical and Applied Climatology*, *122*(3), 531–541. https://doi.org/10.1007/s00704-014-1309-6

Lehnert, M., Savić, S., Milošević, D., Dunjić, J. in Geletič, J. (2021). Mapping local climate zones and their applications in European urban environments: A systematic literature review and future development trends. *ISPRS International Journal of Geo-Information*, *10*(4), 260. https://doi.org/10.3390/ijgi10040260

Lelovics, E., Unger, J., Gál, T. in Gál, C. (2014). Design of an urban monitoring network based on Local Climate Zone mapping and temperature pattern modelling. *Climate Research*, *60*(1), 51–62. https://doi.org/10.3354/cr01220

McKnight, P. E. in Najab, J. (2010). Kruskal-Wallis Test. V I. B. Weiner in W. E. Craighead (ur.), *The Corsini Encyclopedia of Psychology*. John Wiley & Sons.

Mills, G., Bechtel, B., Ching, J., See, L., Feddema, J., Foley, M., Alexander, P. in O'Connor, M. (2015). An introduction to the WUDAPT project [Predstavitev na konferenci]. 9th International Conference on Urban Climates.

Milošević, D., Savić, S., Kresoja, M., Lužanin, Z., Šećerov, I., Arsenović, D., Dunjić, J. in Matzarakis, A. (2022). Analysis of air temperature dynamics in the "local climate zones" of Novi Sad (Serbia) based on long-term database from an urban meteorological network. *International Journal of Biometeorology*, *66*(2), 371–384. https://doi.org/10.1007/s00484-020-02058-w

MKGP [Ministrstvo za kmetijstvo, gozdarstvo in prehrano]. (2023). *Grafični podatki RABA za celo Slovenijo* [Prostorski podatki]. https://rkg.gov.si/vstop/

Mohite, S. in Surawar, M. (2024). Assessing pedestrian thermal comfort to improve walkability in the urban tropical environment of Nagpur city. *Geographica Pannonica*, *28*(1), 71–84. https://doi.org/10.5937/gp28-48166

Ogrin, D. (2015). Long-term air temperature changes in Ljubljana (Slovenia) in comparison to Trieste (Italy) and Zagreb (Croatia). *Moravian Geographical Reports*, *23*(3), 17–26. https://doi.org/10.1515/mgr-2015-0014

Ogrin, D. in Krevs, M. (2015). Assessing urban heat island impact on long-term trends of air temperatures in Ljubljana. *Dela*, *2015*(43), 41–59. https://doi.org/10.4312/dela.43.3.41-59

Ogrin, M., Lampič, B., Svetlin, D., Štaut, L. in Stefanovski, S. (2022). *Toplotni otok mesta Ljubljana, zaključno poročilo (neobjavljeno)*. UL FF.

Ogrin, M., Svetlin, D., Stefanovski, S. in Lampič, B. (2023). Assessment of winter urban heat island in Ljubljana, Slovenia. *Meteorology*, *2*(2), 222–238. https://doi.org/10.3390/meteorology2020014

Oke, T. R. (2002). *Boundary layer climates*. (2nd ed). Routledge. https://doi.org/10.4324/9780203407219

Olofsson, P., Foody, G. M., Herold, M., Stehman, S. V., Woodcock, C. E. in Wulder, M. A. (2014). Good practices for estimating area and assessing accuracy of land change. *Remote Sensing of Environment*, *148*, 42–57. https://doi.org/10.1016/j.rse.2014.02.015

Pipenbaher, N., Ivajnšič, D., Žiberna, I., Donša, D., Kaligarič, M., Škornik, S., Kajfež Bogataj, L., Črepinšek, Z. in Grujić, V. J. (2020). Letna dinamika pojava mestnega toplotnega otoka v malem urbanem sistemu. *Revija za geografijo*, *15*(2), 91–104.

Qian, S., Peng, T., He, R., Chen, J., Zhang, X., Nazir, M. S. in Zhang, C. (2025). A novel ensemble framework based on intelligent weight optimization and multi-model fusion for air quality index prediction. *Urban Climate*, *59*, 102233. https://doi.org/10.1016/j.uclim.2024.102233

Qiu, C., Mou, L., Schmitt, M. in Zhu, X. X. (2019). Local climate zone-based urban land cover classification from multi-seasonal Sentinel-2 images with a recurrent residual network. *ISPRS Journal of Photogrammetry and Remote Sensing*, *154*, 151–162. https://doi.org/10.1016/j.isprsjprs.2019.05.004

Ribeiro, I., Martilli, A., Falls, M., Zonato, A. in Villalba, G. (2021). Highly resolved WRF-BEP/BEM simulations over Barcelona urban area with LCZ. *Atmospheric Research*, *248*, 105220. https://doi.org/10.1016/j.atmosres.2020.105220

Savić, S., Milošević, D., Lazić, L., Marković, V., Arsenović, D. in Pavić, D. (2013). Classifying urban meteorological stations sites by „local climate zones": preliminary results for the city of Novi Sad (Serbia). *Geographica Pannonica*, *17*(3), 60–68. https://doi.org/10.1016/j.isprsjprs.2019.05.004

Shen, X., Liu, B. in Lu, X. (2017). Effects of land use/land cover on diurnal temperature range in the temperate grassland region of China. *Science of The Total Environment*, *575*, 1211–1218. https://doi.org/10.1016/j.scitotenv.2016.09.187

Silva, B. B. da, Braga, A. C., Braga, C. C., Oliveira, L. M. M. de, Montenegro, S. M. G. L. in Barbosa Junior, B. (2016). Procedures for calculation of the albedo with OLI-Landsat 8 images: Application to the Brazilian semi-arid. *Revista Brasileira de Engenharia Agrícola e Ambiental*, *20*(1), 3–8. http://dx.doi.org/10.1590/1807-1929/agriambi.v20n1p3-8v

Sobrino, J. A., Jiménez-Muñoz, J. C. in Paolini, L. (2004). Land surface temperature retrieval from LANDSAT TM 5. *Remote Sensing of Environment*, *90*(4), 434–440. https://doi.org/10.1016/j.rse.2004.02.003

Stewart, I. D. in Oke, T. R. (2012). Local climate zones for urban temperature studies. *Bulletin of the American Meteorological Society*, *93*(12), 1879–1900. https://doi.org/10.1175/BAMS-D-11-00019.1

Tian, X., Zhang, H., Liu, L., Huang, J., Liu, L. in Liu, J. (2024). Establishment of LCZ-based urban building energy consumption dataset in hot and humid subtropical regions through a bottom-up method. *Applied Energy*, *368*, 123491. https://doi.org/10.1016/j.apenergy.2024.123491

Unger, J., Lelovics, E. in Gál, T. (2014). Local Climate Zone mapping using GIS methods in Szeged. *Hungarian Geographical Bulletin*, *63*(1), 29–41. https://doi.org/10.15201/hungeobull.63.1.3

USGS [U.S. Geological Survey]. (2022). *LC08_L1TP_191028_20220720_20220726_02_T1* [Prostorski podatki]. https://earthexplorer.usgs.gov/

USGS. (2023a). *LC08_L1TP_190028_20230630_20230711_02_T1* [Prostorski podatki]. https://earthexplorer.usgs.gov/

USGS. (2023b). *LC09_L1TP_190028_20230708_20230708_02_T1* [Prostorski podatki]. https://earthexplorer.usgs.gov/

USGS. (2023c). *LC09_L1TP_191028_20230715_20230715_02_T1* [Prostorski podatki]. https://earthexplorer.usgs.gov/

Wang, R., Wang, M., Ren, C., Chen, G., Mills, G. in Ching, J. (2024). Mapping local climate zones and its applications at the global scale: A systematic review of the last decade of progress and trend. *Urban Climate*, *57*, 102129. https://doi.org/10.1016/j.uclim.2024.102129

Yang, X., Peng, L. L. H., Chen, Y., Yao, L. in Wang, Q. (2020). Air humidity characteristics of local climate zones: A three-year observational study in Nanjing. *Building and Environment*, *171*, 106661. https://doi.org/10.1016/j.buildenv.2020.106661

Združeni narodi. (2019). *World urbanization prospects: The 2018 revision (ST/ESA/SER.A/420).* Združeni narodi. https://population.un.org/wup/assets/WUP-2018-Report.pdf

Zhou, X., Okaze, T., Ren, C., Cai, M., Ishida, Y. in Mochida, A. (2020). Mapping local climate zones for a Japanese large city by an extended workflow of WUDAPT Level 0 method. *Urban Climate*, *33*, 100660. https://doi.org/10.1016/j.uclim.2020.100660

Žiberna, I. (2006). Trendi temperatur zraka v Mariboru kot posledica razvoja mestnega toplotnega otoka. *Revija za geografijo*, *1*(1), 81–98.

Žiberna, I. in Ivajnšič, D. (2022). *Sezonski režim površinskega mestnega toplotnega otoka v Mariboru*. V D. Donša, V. J. Grujić in N. Pipenbaher (ur.), *Primeri prostorskih analiz vplivov podnebnih sprememb: Monografija v okviru projekta Preprečevanje toplotnega stresa v urbanih sistemih v luči podnebnih sprememb (ARRS J7-1822)*. University of Maribor Press. https://doi.org/10.18690/um.fnm.8.2022

Žiberna, I., Pipenbaher, N., Donša, D., Škornik, S., Kaligarič, M., Bogataj, L. K., Črepinšek, Z., Grujić, V. J. in Ivajnšič, D. (2021). The impact of climate change on urban thermal environment dynamics. *Atmosphere*, *12*(9), 1159. https://doi.org/10.3390/atmos12091159

Tim Gregorčič*, Stevan Savić**, Blaž Repe*, Matej Ogrin*

MAPPING LOCAL CLIMATE ZONES OF LJUBLJANA: A DUAL METHODOLOGICAL APPROACH

COBISS 1.01
DOI: 10.4312/GRKP6310

Abstract

The Local Climate Zone (LCZ) framework was introduced to facilitate standardised research in the field of urban climate and other related scientific disciplines. This study presents the LCZ classification of Ljubljana, employing two methods: Cellular Automata and WUDAPT. Their effectiveness was evaluated by explaining spatial variations in land surface temperature and canopy urban heat islands, as well as through expert judgement. The results of the WUDAPT method are considered more representative, thus providing a robust foundation for future urban climate research.

Keywords: local climate zones (LCZ), WUDAPT, cellular automata, urban climate, micrometeorological classification

*Department of Geography, Faculty of Arts, University of Ljubljana, Aškerčeva 2, SI-1000 Ljubljana, Slovenia
**Department of Geography, Tourism and Hotel Management, Faculty of Sciences, University of Novi Sad, Trg Dositeja Obradovića 3, RS-21000 Novi Sad, Serbia
e-mail: tim.gregorcic@ff.uni-lj.si; stevan.savic@dgt.uns.ac.rs, blaz.repe@ff.uni-lj.si, matej.ogrin@ff.uni-lj.si
ORCID: 0009-0006-9767-9428 (T. Gregorčič), 0000-0002-4297-129X (S. Savić), 0000-0002-5530-4840 (B. Repe), 0000-0002-4742-3890 (M. Ogrin)

1 INTRODUCTION

By the middle of the 21st century, more than 60% of the global population is expected to reside in urban areas (United Nations, 2019). Although urbanisation in most European countries is not anticipated to progress as rapidly as in many countries of the Global South, this does not necessarily imply fewer emerging urban challenges. European cities still warrant study from multiple perspectives due to challenges associated with environmental changes, including climate change, as well as an ageing population, technological advancements, and social inequalities. As climate is one of the most critical factors influencing quality of life, urban climate studies are essential for the development of liveable cities of the future. Urban climate studies frequently focus on topics such as air quality (Qian et al., 2025), indoor and outdoor human thermal comfort (Mohite & Surawar, 2024; Hu et al., 2023; Žiberna et al., 2021), the urban heat island (Assaf & Assaad, 2024; Ogrin, 2015; Ogrin & Krevs, 2015; Ogrin et al., 2023; Pipenbaher et al., 2020; Žiberna, 2006; Žiberna & Ivajnšič, 2022), and local climate zones (LCZs) (Ogrin et al., 2023; Wang, Wang, et al., 2024; Žiberna et al., 2021). LCZs were defined by Stewart and Oke (2012, p. 1884) as "regions of uniform surface cover, structure, material, and human activity that span hundreds of metres to several kilometres in horizontal scale." The LCZ classification scheme comprises 10 predominantly built types and 7 predominantly natural types, with each type characterised by specific structural and cover properties (Figure 1). While this is not the only framework for urban climate zoning, it is the most widely used and is therefore regarded as the standard in urban climate studies (Lehnert et al., 2021). LCZs are not only studied in isolation but are often used as a foundation for analysing the spatial dynamics of other urban phenomena. Consequently, the development of robust LCZ classifications for population centres is critical, as they can underpin applied urban climate studies aimed at enhancing urban resilience in the context of climate change.

Over the years, numerous LCZ mapping methodologies have been proposed, which can be categorised into four groups: (a) remote sensing imagery-based, (b) GIS-based, (c) combined methods, and (d) expert knowledge-based approaches (Lehnert et al., 2021). Remote sensing imagery-based approaches classify LCZs using supervised classification methods applied to satellite or airborne surface observation data, making this the most commonly employed method (Huang et al., 2023). For instance, the World Urban Database and Access Portal Tools (WUDAPT) project was developed "for the acquisition, storage and dissemination of climate relevant data on the physical geographies of cities worldwide" (Mills et al., 2015). Among other functionalities, WUDAPT facilitates LCZ mapping using random forest algorithms and data derived from satellite surface observations, making it the most widely adopted approach. For example, Qiu et al. (2019) classified LCZs in cities such as Paris, Milan, and London using WUDAPT.

Figure 1: Description of local climate zone types.

Source: Demuzere et al., 2021.

GIS-based classification approaches determine LCZs by calculating physical parameters, defining basic spatial units, classifying LCZs, and evaluating classification results (Huang et al., 2023). An example of this approach is the LCZ classification of Szeged (Unger et al., 2014).

Combined methods, which integrate remote sensing imagery and GIS-based approaches, are often employed to address gaps in surface morphological or land cover data, offer alternative approaches for comparison with GIS-based methods, and enhance the sensitivity of remote sensing imagery-based classifications (Lehnert et al., 2021). For instance, Zhou et al. (2020) utilised this combined approach to map LCZs in the Japanese city of Sendai.

Expert knowledge-based methods rely on local expertise, often informed by metadata from specific meteorological station sites within an urban meteorological network, which represent distinct micro- or local conditions (Lehnert et al., 2021). However, as urban meteorological networks are uncommon, this approach is rarely applied. One example is the study conducted in Novi Sad, where nine LCZs were identified as potential locations for 28 future urban meteorological stations (Savić et al., 2013). Similarly, this approach was used in the LCZ classification of Olomouc (Lehnert et al., 2015).

Although LCZ mapping has been conducted for numerous cities in Central and Southeastern Europe, an in-depth study of Ljubljana's LCZs remains absent. Ljubljana has a tradition of studying the urban heat island (UHI) effect spanning over 20 years. The first comprehensive UHI study dates back to 2000 (Jernej, 2000), when the established methods for determining UHI differed from those used today. Ciglič and Komac (2014) conducted a remote sensing analysis of the surface UHI in Ljubljana and contributed to the Atlas of Central European Cities with UHI. Between 2020 and 2022, the Department of Geography at the University of Ljubljana, Faculty of Arts, conducted a comprehensive UHI study of Ljubljana. This study incorporated field measurements, a network of stationary monitoring stations, and satellite imagery to determine the "local temperature zones" (LTZs) (Ogrin et al., 2022). LTZs partially originated from LCZs. However, as the methodology only partially adhered to the framework of Stewart and Oke (2012), the resulting classes could not be classified as LCZs nor compared with similar studies. In an attempt to address this gap which is just an example of many similar cases, Demuzere et al. (2022) employed the WUDAPT method to produce a global LCZ map. While Ljubljana was included in their study, the results for the built types (LCZ 1–10) were overly generalised due to the lack of explicitly defined training areas in Ljubljana. Additionally, their findings were not evaluated for their ability to explain spatial variations in urban climate parameters such as UHI or land surface temperature (LST).

Thus, the purpose of this study was to develop a LCZ map of Ljubljana as defined by Stewart and Oke (2012). The specific objectives were to: (G1) create the spatial data required to classify LCZs, (G2) classify the LCZs of Ljubljana using cellular automata (CA), (G3) classify the LCZs of Ljubljana using the WUDAPT method, and

(G4) evaluate the outcomes of both methodologies based on their ability to explain the spatial variability of land surface temperature (LST) and canopy urban heat island (CUHI), as well as the expert judgement of the authors.

2 METHODOLOGY

2.1 Spatial Data Derivation

The boundaries of the study area correspond to those defined by the Geodetic Administration of the Republic of Slovenia in the settlements layer of the Spatial Unit Register (SMARS, 2023c). Unless stated otherwise, the spatial data required for the classification were created using ArcGIS Pro. For the classification of LCZs, the following spatial data layers were produced:

- Pervious surface fraction (PSF),
- Building surface fraction (BSF),
- Impervious surface fraction (ISF),
- Sky view factor (SVF),
- Height of roughness elements (HRE),
- Aspect ratio (AR),
- Terrain roughness class (TRC), and
- Surface albedo (SA).

Pervious surface fraction: The pervious surface fraction layer (the ratio of pervious plan area—bare soil, vegetation, water—to total plan area, in %) was created using multiple data sources. A composite image was generated from red, green, blue, and near-infrared orthophoto bands captured in 2015 (SMARS, 2015). This composite image was employed to classify built-up and other areas using the Supervised Classification method within the ArcGIS Pro Classification Wizard. Separately, the NDVI was calculated from the red and near-infrared orthophoto bands (Goward et al., 1991) and reclassified into two classes: areas with vegetation (NDVI ≥ 0.2) and areas without vegetation (NDVI < 0.2). The built-up areas identified through supervised classification and the vegetated areas derived from the NDVI calculation were then merged with selected classes from the national land use layer (MAFF, 2023), as presented in Table 1. The resulting final layer represented pervious surface fraction and included all built-up areas (building surface fraction and pervious surface fraction combined). The quality of the classification was assessed using Cohen's kappa (Olofsson et al., 2014). With a kappa value of 0.93, the classification was considered to exhibit near-perfect agreement with the real-world situation (Chien-Ta et al., 2015). In the subsequent step, a fishnet with a polygon width of 100 m was created, representing the spatial resolution of the CA LCZ classification. This resolution was selected based on similar international studies (Demuzere et al., 2021; Geletič & Lehnert, 2016; Huang et al., 2023; Kim et al., 2021). The pervious surface fraction was then calculated and assigned to each polygon.

Table 1: Classes of national land use layer used for the identification of pervious surfaces.

Code	Land-use type	Code	Land-use type	Code	Land-use type
1100	Arable land	1240	Other permanent crops	1600	Uncultivated farmland
1180	Farmland with forest overgrowth	1300	Permanent grassland	1800	Farmland with forest overgrowth
1211	Vineyard	1321	Swampy meadow	2000	Forest
1212	Nursery	1410	Old-field succession	4220	Other swampy land
1221	Intensive orchard	1420	Forest plantation	7000	Water
1222	Extensive or meadow orchard	1500	Trees and shrubs		

Source: MAFF, 2023.

Building surface fraction: The calculation of building surface fraction layer (the ratio of building plan area to total plan area, in %) was based on the Real Estate Cadastre (REC) from 2023 (SMARS, 2023b). In the later stages of the methodology, LiDAR data captured between 2014 and 2015 (SEA, 2023) was utilised. To ensure comparability with the LiDAR data, all buildings constructed after 2015 were excluded from the REC dataset. A normalised digital surface model (nDSM) was derived from the LiDAR data at a spatial resolution of 1 m, and the average building height was calculated. Polygons with an average height of 2.5 m or less were removed. In some cases, the nDSM still included the heights of buildings that had been demolished after 2015 and were already excluded from the REC. Since such occurrences were rare, this error was deemed negligible, and no adjustments were made to the LiDAR data. The REC area for each fishnet polygon was calculated, and building surface fraction was derived in the final stage based on this information.

Impervious surface fraction: After pervious surface fraction and building surface fraction, the impervious surface fraction layer (the ratio of impervious plan area—paved surfaces, rock—to total plan area, in %) was then calculated using Formula 1.

Formula 1: $ISF = 100 - PSF - BSF$

Sky View Factor: For the sky view factor layer (the ratio of the visible sky hemisphere from ground level to that of an unobstructed hemisphere), a DSM incorporating data on relief, high vegetation, and building heights was created. This DSM was generated from the LiDAR data at a spatial resolution of 1 m. The sky view factor layer was then calculated from the DSM using SAGA GIS software. Subsequently, all areas except the ground were removed from the sky view factor layer based on values greater than 0 in the newly derived nDSM. In the final stage, the average sky view factor value was calculated for each polygon in the fishnet.

Height of roughness elements: This variable includes all spatial elements with height. Where the value of pervious surface fraction was less than 90% and the value of impervious surface fraction was between 90% and 10%, data on building heights was required. Where the value of pervious surface fraction was 90% or more, or the value of impervious surface fraction was 90% or more, data on the height of all vegetation, not just trees, was considered (Stewart & Oke, 2012). For building heights, the nDSM layer created during the calculation of building surface fraction was used. For the height of all vegetation, a new nDSM layer was created from the ground, low, medium, and high vegetation LiDAR categories. Based on the described Boolean logic, the average value of the appropriate nDSM, excluding cells with a value of 0, was calculated for each polygon in the fishnet.

Aspect ratio: Aspect ratio is defined as the mean height-to-width ratio of street canyons or building spacing (where the value of pervious surface fraction is less than 90% and the value of impervious surface fraction is between 90% and 10%) or tree spacing (where the value of pervious surface fraction is 90% or more, or the value of impervious surface fraction is 90% or more) (Stewart & Oke, 2012). While data on building and tree heights were already available, it was still necessary to calculate width data. To achieve this, vectorised areas of buildings or tree canopies were excluded from the fishnet. Using an ArcGIS Pro plugin called XTools Pro, the average width of the intermediate space was calculated using the *Polygon Width* tool. The point-based results were then averaged to the polygonal grid to calculate the height-to-width ratio.

Terrain roughness class: terrain roughness classes are derived from the roughness length (Z_0), which is a measure of the aerodynamic roughness of a surface, defined as the height at which the neutral wind profile near the ground extrapolates to zero (Oke, 2002). Z_0 is calculated using Formula 2, where f_0 is the empirical coefficient (0.1) and $\overline{Z_H}$ represents the average height of surface elements (Hammond et al., 2012). For terrain roughness classes, $\overline{Z_H}$ within the fishnet was calculated from the nDSM, excluding cells with a value of 0. The nDSM was derived from LiDAR classes for low, medium, and high vegetation, as well as buildings. Values of Z_0 were then reclassified into terrain roughness classes based on Table 2.

$$Z_0 = f_0\overline{Z_H}$$

(Formula 2)

Table 2: Definition of terrain roughness classes.

Z_0	Terrain roughness class
0.0000–0.0020	1
0.0021–0.0050	2
0.0051–0.0300	3
0.0301–0.1000	4
0.1001–0.2500	5
0.2501–0.5000	6
0.5001–1.0000	7
> 1.0000	8

Source: Davenport et al., 2000.

Surface albedo: The surface albedo layer (the ratio of the amount of solar radiation reflected by a surface to the amount received by it) was calculated using Landsat satellite imagery from 20 July 2022 (USGS, 2022). The methodology described by Silva et al. (2016), Chander & Markham (2003) and Allen et al. (2002) was followed. Additionally, their approach was enhanced by calculating the air pressure correction factor (the difference between the modelled and measured values from the meteorological station Ljubljana Bežigrad) and applying it to the modelled air pressure result. Maps of all derived spatial classification input data are shown in Figure 2.

Figure 2: Maps of the derived spatial classification input data.

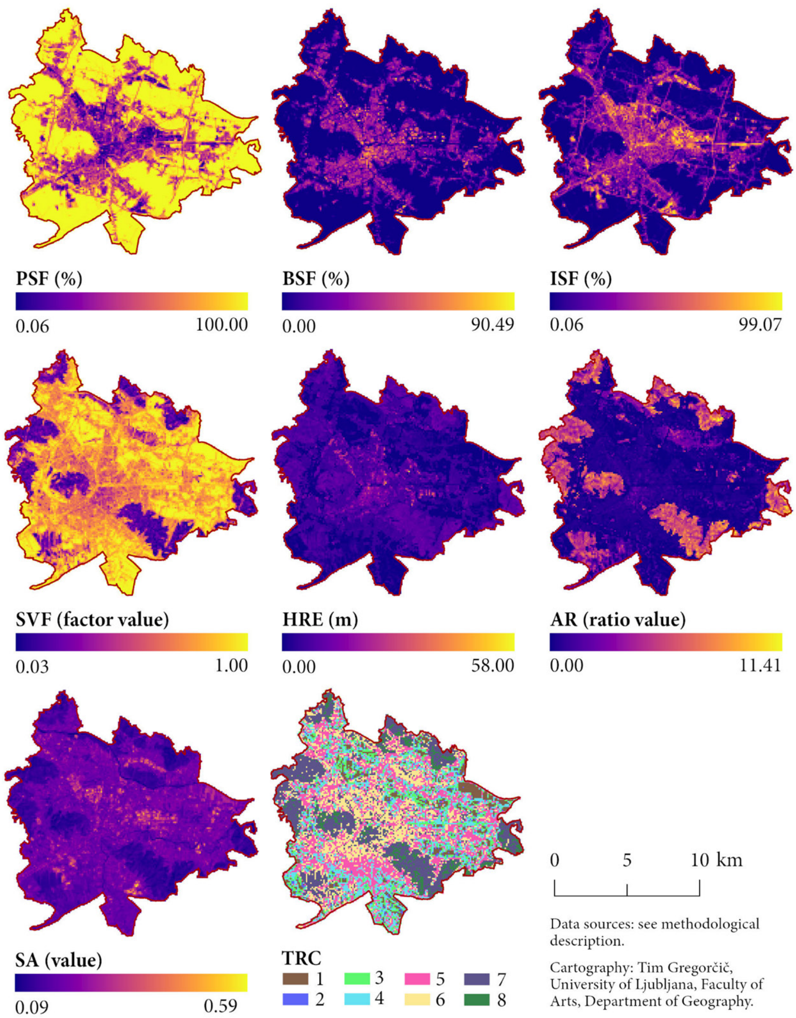

2.2 Standardisation of Derived Explanatory Variables

The classification of LCZs required the standardisation of all data layers created in Section 2.1 for each LCZ according to their quantitative definitions. The layers were standardised on a scale from 0 to 1, with a value of 1 assigned to cells belonging to a particular LCZ as defined in Table 3. Standardisation was performed using a combined fuzzification process (increasing and decreasing) in TerrSet software. The boundaries for the start of the increase and the end of the decrease were defined according to the interval characterising the LCZ for the selected variable (Figure 3, Table 3) (Unger et al., 2014). In total, 136 standardised layers (8 for each LCZ) were created. Using ArcGIS Pro, all 8 layers for each LCZ were merged into a single layer using the Fuzzy Overlay tool. The Boolean logic "AND" option was applied to minimise "value trading" between layers (Estacio et al., 2019).

Figure 3: Explanatory variables standardisation model.

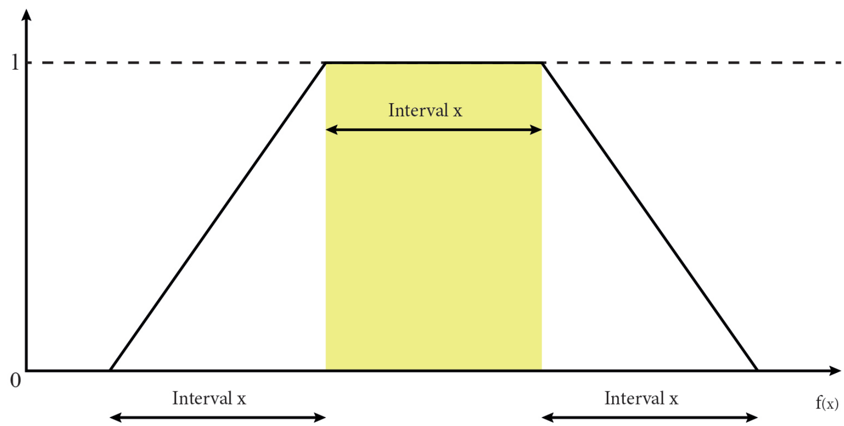

Source: Unger et al., 2014.

Table 3: Quantitative description of LCZ classes for each explanatory variable.

LCZ	SVF	AR	BSF	ISF	PSF	HRE	TRC	SA
LCZ 1	0.2–0.4	> 2	40–60	40–60	< 10	> 25	8	0.10–0.20
LCZ 2	0.3–0.6	0.75–2	40–70	30–50	< 20	10–25	6–7	0.10–0.20
LCZ 3	0.2–0.6	0.75–1.5	40–70	20–50	< 30	3–10	6	0.10–0.20
LCZ 4	0.5–0.7	0.75–1.25	20–40	30–40	30–40	> 25	7–8	0.12–0.25

LCZ	SVF	AR	BSF	ISF	PSF	HRE	TRC	SA
LCZ 5	0.5–0.8	0.3–0.75	20–40	30–50	20–40	10–25	5–6	0.12–0.25
LCZ 6	0.6–0.9	0.3–0.75	20–40	20–50	30–60	3–10	5–6	0.12–0.25
LCZ 7	0.2–0.5	1–2	60–90	< 20	< 30	2–4	4–5	0.15–0.35
LCZ 8	>0.7	0.1–0.3	30–50	40–50	< 20	3–10	5	0.12–0.25
LCZ 9	> 0.8	0.1–0.25	10–20	< 20	60–80	3–10	5–6	0.12–0.25
LCZ 10	0.6–0.9	0.2–0.5	20–30	20–40	40–50	5–15	5–6	0.12–0.20
LCZ A	< 0.4	> 1	< 10	< 10	> 90	3–30	8	0.10–0.20
LCZ B	0.5–0.8	0.25–0.75	< 10	< 10	> 90	3–15	5–6	0.15–0.25
LCZ C	0.7–0.9	0.25–1.0	< 10	< 10	> 90	< 2	4–5	0.15–0.30
LCZ D	> 0.9	< 0.1	< 10	< 10	> 90	< 1	3–4	0.15–0.25
LCZ E	> 0.9	< 0.1	< 10	> 90	< 10	< 0.25	1–2	0.15–0.30
LCZ F	> 0.9	< 0.1	< 10	< 10	> 90	< 0.25	1–2	0.20–0.35
LCZ G	> 0.9	< 0.1	< 10	< 10	> 90	–	1	0.02–0.10

Source: Stewart & Oke, 2012.

2.3 Classification of Local Climate Zones

For the classification of LCZs, we employed two different methodologies: CA and WUDAPT. For the CA-based classification of LCZs, we utilised Python code that was written and applied by Estacio et al. (2019) in their classification study. The final standardised layers from Section 2.2, representing all LCZs, were used as input data, with the code executed within ArcGIS Pro.

For the classification of LCZs using the WUDAPT method, we first created training areas. These areas were delimited based on the same final standardised layers used for the initial classification. Parts of the areas within these layers with values of 0.9 or higher were considered suitable. In the case of LCZ 8, training zones were exceptionally defined, despite the low values of the standardised layer, because, according to the definition, this type of LCZ comprises a significant proportion of the study area (e.g., BTC City Ljubljana, Rudnik shopping area, Industrial Zone Šiška, etc.). The training areas were then uploaded to the WUDAPT platform in KML format, and the classification process was carried out using data from Landsat 8, Sentinel 1, Sentinel 2, and other sources (Demuzere et al., 2021). In the final step, the raw WUDAPT result was generalised using the methodology for generalising classified raster imagery (*Generalization of Classified Raster Imagery—ArcMap | Documentation*, n.d.).

2.4 Quality Assessment of the Classification Results

The decision on the most appropriate final classification was based on a combination of quantitative evaluation and expert opinion. Quantitative evaluation was conducted through each classification's ability to explain spatial variation in LST and summer CUHI. We calculated the average LST layer from Landsat 8 and Landsat 9 data, following the methodologies of Sobrino et al. (2004) and Avdan & Jovanovska (2016). The average layer was calculated from the results of June 30, July 8, and July 15, 2023 (USGS, 2023c, 2023b, 2023a). The summer CUHI layer was obtained from Ogrin et al. (2023). For each class of both classifications, 17.84 random sampling points per square kilometre were generated, with a maximum of 1,000 random sampling points for the class with the largest area. In the next step, the LST and CUHI layers were sampled using these points. Due to the non-normal distribution of the data, non-parametric Kruskal–Wallis and Dunn's post-hoc tests (McKnight & Najab, 2010) were used to analyse LST and CUHI differences between classes. Due to the limitations of the selected statistical methods, only LCZ types where at least 30 points were generated were assessed.

3 RESULTS

The result of the LCZ classification using the CA method is presented in Figure 4. This method identified four built LCZ types (LCZ 2, LCZ 5, LCZ 6, LCZ 9) and five natural LCZ types (LCZ A, LCZ B, LCZ C, LCZ E, LCZ F). Among these, LCZ 2, LCZ 5, LCZ 6, LCZ A, LCZ C, and LCZ F were considered for quantitative analysis. When analysing the difference in CUHI values between the classes, the result of the Kruskal-Wallis test was statistically significant ($p < 0.05$). Consequently, we rejected the null hypothesis (H_0) that the groups are subsets of the same population and concluded that there is evidence to support the alternative hypothesis (H_a) that at least one group differs from the others (Table 4). The Dunn's post-hoc test (Table 5) revealed that the medians are statistically significantly different in all cases of LCZ pairs ($p < 0.05$), except between LCZ 2 and LCZ 5. Box plots in Figure 5 show the data distribution of CUHI values.

Figure 4: Local climate zones classification using the CA method.

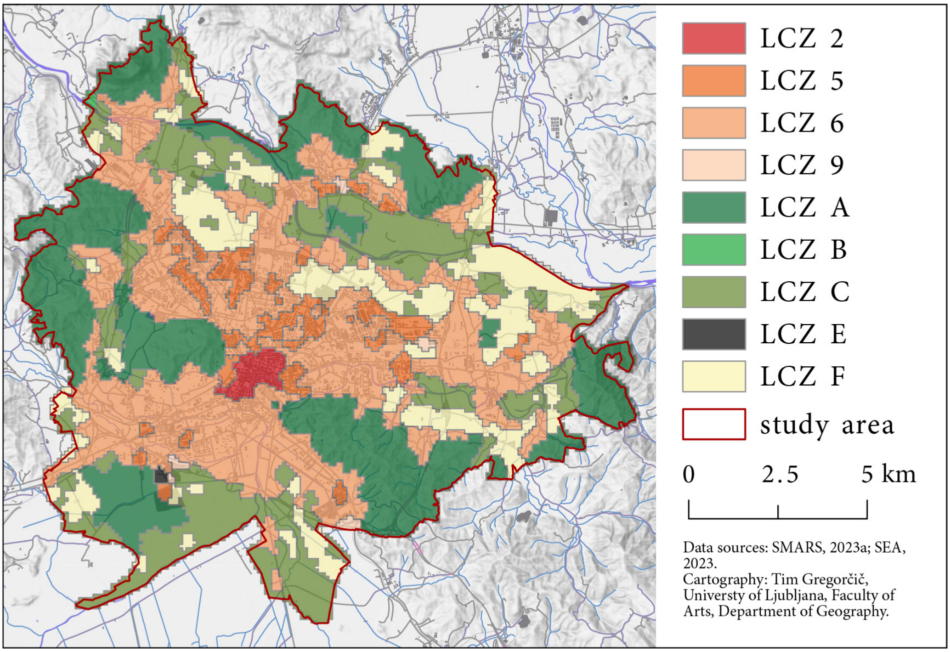

Table 4: Kruskal-Wallis test result for CUHI differences among LCZs using the CA method.

Kruskal-Wallis rank sum test		
Kruskal-Wallis chi-squared	Df	Sig.
1485.5	5	< 0.05

Table 5: Dunn's post-hoc test result for CUHI differences among LCZ pairs using the CA method.

Dunn's post-hoc test (Bonferroni)						
		LCZ 2	LCZ 5	LCZ 6	LCZ A	LCZ C
LCZ 5	z	2.02				
	p adjusted	0.33				
LCZ 6	z	5.60	7.56			
	p adjusted	<0.05	<0.05			

Dunn's post-hoc test (Bonferroni)							
		LCZ 2	LCZ 5	LCZ 6	LCZ A	LCZ C
LCZ A	z	9.74	16.45	16.27		
	p adjusted	<0.05	<0.05	<0.05		
LCZ C	z	14.33	25.61	30.71	15.62	
	p adjusted	<0.05	<0.05	<0.05	<0.05	
LCZ F	z	12.25	20.77	21.89	8.32	−5.69
	p adjusted	<0.05	<0.05	<0.05	<0.05	<0.05

Figure 5: CUHI data distribution for each class of LCZ classification using the CA method.

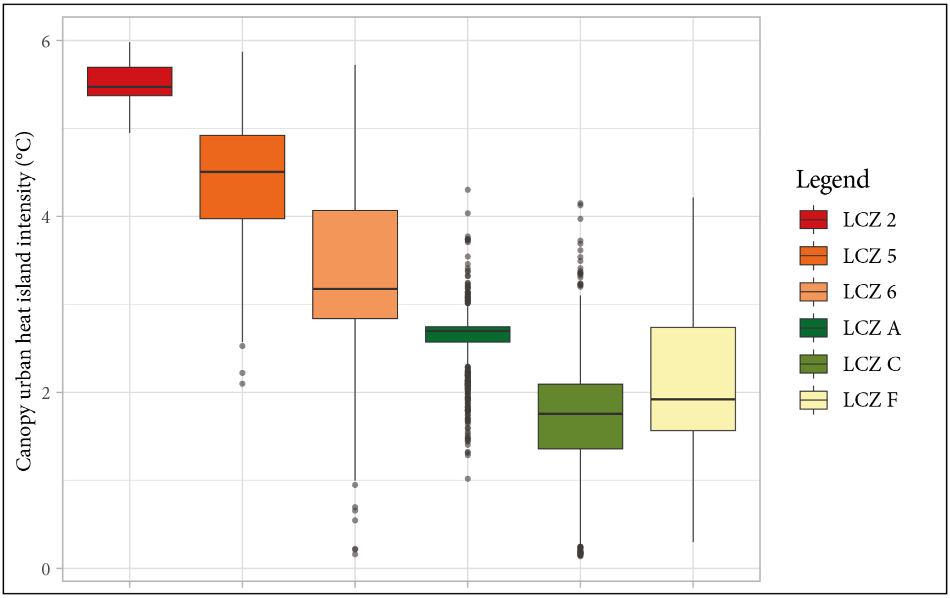

When analysing the difference in LST values between the classes, we again rejected H_0 of the Kruskal-Wallis test ($p < 0.05$) (Table 6). The same relationships between LCZ pairs observed in the case of CUHI were also identified for LST in the results of the Dunn's post-hoc test (Table 7). The relationship between LCZ 2 and LCZ 5 was the only pair for which no significant difference was found. Figure 6 illustrates the distribution of LST values using box plots.

Table 6: Kruskal-Wallis test result for LST differences among LCZs using the CA method.

Kruskal-Wallis rank sum test		
Kruskal-Wallis chi-squared	Df	Sig.
2200.4	5	< 0.05

Table 7: Dunn's post-hoc test result for LST differences among LCZ pairs using the CA method.

Dunn's post-hoc test (Bonferroni)						
		LCZ 2	LCZ 5	LCZ 6	LCZ A	LCZ C
LCZ 5	z	2.02				
	p adjusted	0.33				
LCZ 6	z	5.60	7.56			
	p adjusted	<0.05	<0.05			
LCZ A	z	9.74	16.45	16.27		
	p adjusted	<0.05	<0.05	<0.05		
LCZ C	z	14.33	25.61	30.71	15.62	
	p adjusted	<0.05	<0.05	<0.05	<0.05	
LCZ F	z	12.25	20.77	21.89	8.32	–5.69
	p adjusted	<0.05	<0.05	<0.05	<0.05	<0.05

Figure 6: LST data distribution for each class of LCZ classification using the CA method.

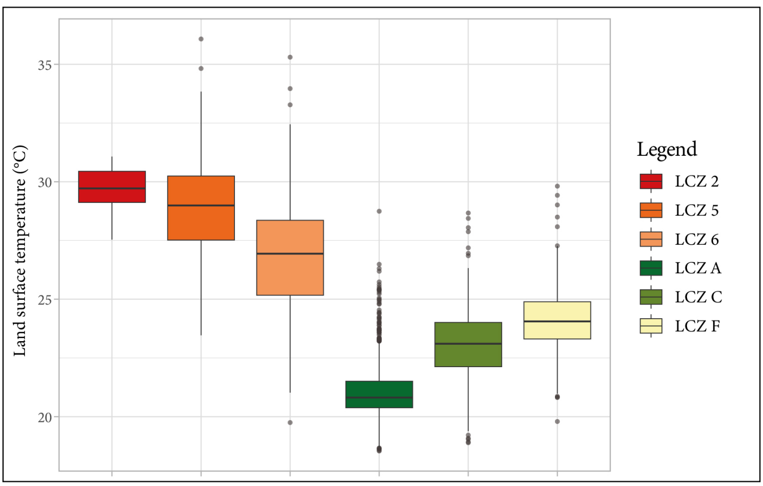

The result of the LCZ classification using the WUDAPT method is shown in Figure 7. Using this method, we identified four built LCZ types (LCZ 2, LCZ 5, LCZ 6, LCZ 8) and five natural LCZ types (LCZ A, LCZ C, LCZ D, LCZ F, LCZ G). Unlike the CA method, WUDAPT provides different metrics to evaluate the performance of the classification based on the training samples (Figure 8). We consider the overall accuracy of the classification to be good, as 76% of training pixels were classified correctly (OA = 0.76). The overall accuracy of urban LCZs (OAu) was 0.70, while the overall accuracy of the built versus natural LCZ classes (OAbu) was 0.99, meaning that only 1% of urban LCZ training pixels were missclassified into one of the natural LCZ classes and vice versa. The overall weighted accuracy (OAw), which accounts for the (dis)similarity between LCZ types and penalises confusion between dissimilar types more than confusion between similar types, was 0.95 (Demuzere et al., 2021). Class-wide accuracy, evaluated using the F1 metric, was above 0.75 in all cases except for LCZ 5. Therefore, we can generally consider the results to be good (Chicco & Jurman, 2020).

Figure 7: Local climate zones classification using the WUDAPT method.

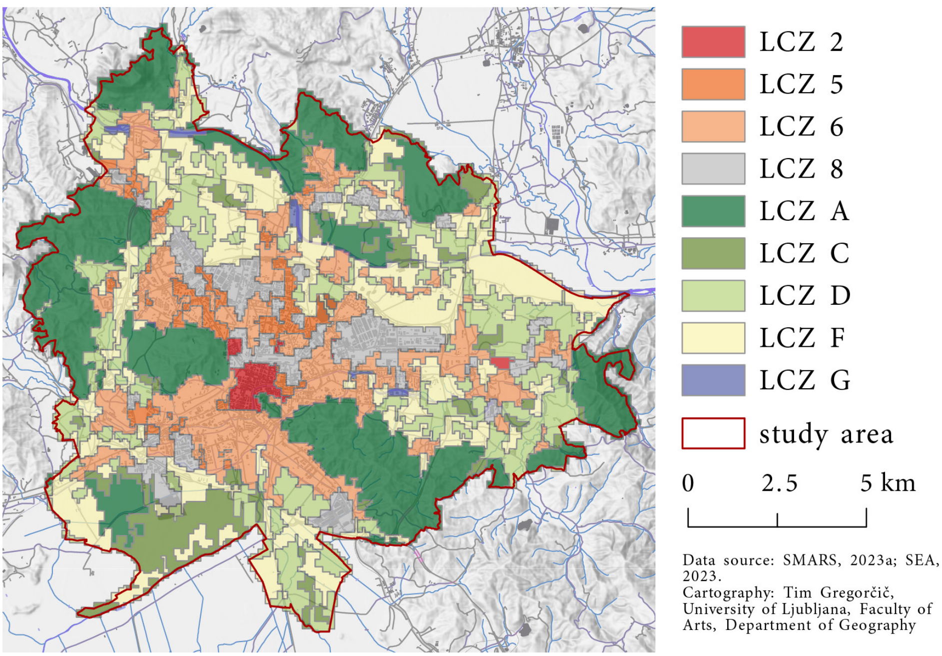

Figure 8: Accuracy assessment of WUDAPT classification result.

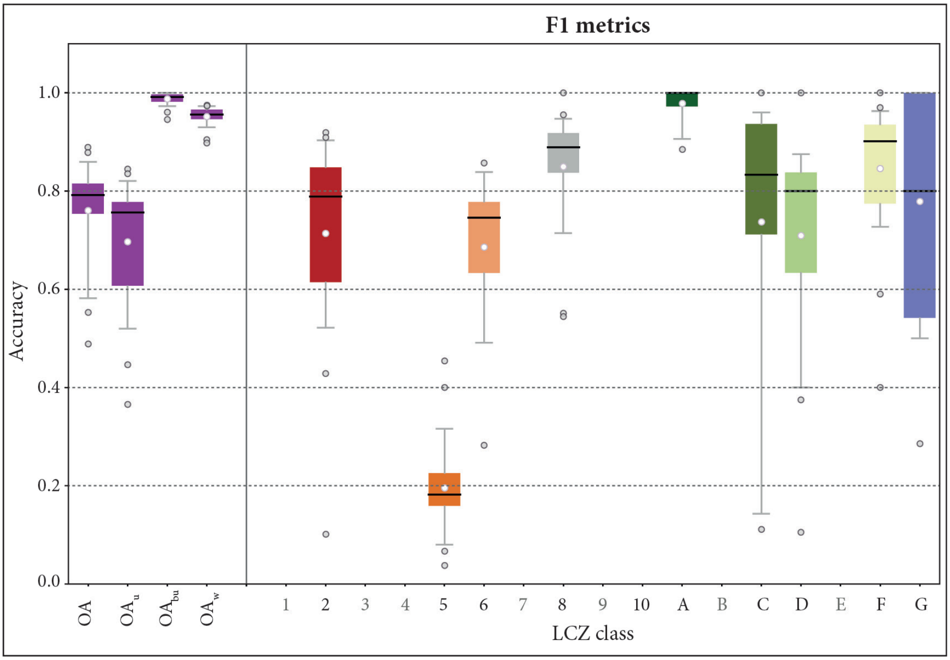

For the CUHI and LST analyses of the WUDAPT classification, LCZ 2, LCZ 5, LCZ 6, LCZ 8, LCZ A, LCZ C, LCZ D, and LCZ F were considered. When analysing the difference in CUHI values between the classes, the result of the Kruskal-Wallis test was statistically significant ($p < 0.05$). Thus, we rejected the null hypothesis (H_0) and concluded that there is evidence to support the alternative hypothesis (H_a) (Table 8). The Dunn's post-hoc test (Table 9) showed that the medians are statistically significantly different in all cases of LCZ pairs ($p < 0.05$), except between LCZ 2 & LCZ 5, LCZ 2 & LCZ 8, LCZ 5 & LCZ 8, and LCZ C & LCZ D. Box plots in Figure 9 show the data distribution of CUHI values.

Table 8: Kruskal-Wallis test result for CUHI differences among LCZs using the WUDAPT method.

Kruskal-Wallis rank sum test		
Kruskal-Wallis chi-squared	Df	Sig.
1440.1	7	< 0.05

Table 9: Dunn's post-hoc test result for CUHI differences among LCZ pairs using the WUDAPT method.

Dunn's post-hoc test (Bonferroni)								
		LCZ 2	LCZ 5	LCZ 6	LCZ 8	LCZ A	LCZ C	LCZ D
LCZ 5	z	1.79						
	p adjusted	1.00						
LCZ 6	z	3.91	2.95					
	p adjusted	<0.05	0.04					
LCZ 8	z	2.50	0.81	−2.940				
	p adjusted	0.18	1.00	0.05				
LCZ A	z	9.38	11.66	16.53	15.72			
	p adjusted	<0.05	<0.05	<0.05	<0.05			
LCZ C	z	12.95	16.12	19.92	19.72	9.33		
	p adjusted	<0.05	<0.05	<0.05	<0.05	<0.05		
LCZ D	z	13.14	17.35	25.63	23.30	11.63	-1.02	
	p adjusted	<0.05	<0.05	<0.05	<0.05	<0.05	1.00	
LCZ F	z	11.66	15.16	22.44	20.50	7.39	-4.27	-4.44
	p adjusted	<0.05	<0.05	<0.05	<0.05	<0.05	<0.05	<0.05

Figure 9: CUHI data distribution for each class of LCZ classification using the WUDAPT method.

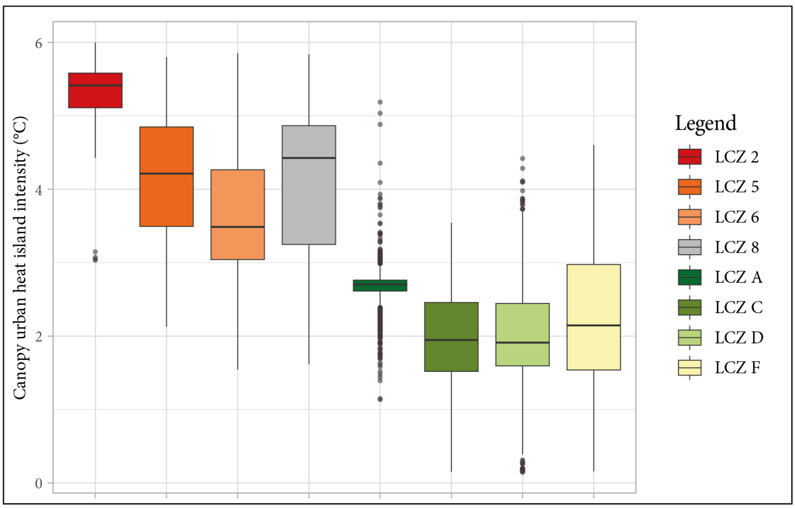

When analysing the difference in LST values between the classes, we again rejected H_0 ($p < 0.05$) (Table 10). Based on Dunn's post-hoc test, we can reject H_0 in all cases except for LCZ 2 & LCZ 5, LCZ 2 & LCZ 6, LCZ 2 & LCZ 8, LCZ 5 & LCZ 6, LCZ 5 & LCZ 8, and LCZ D & LCZ F (Table 11). This means that, in all LCZ combinations, except for the aforementioned, the medians of LST differ significantly from one another. Figure 10 illustrates the distribution of LST values using box plots.

Table 10: Kruskal-Wallis test result for LST differences among LCZs using the WUDAPT method.

Kruskal-Wallis rank sum test		
Kruskal-Wallis chi-squared	Df	Sig.
2273.4	7	< 0.05

Table 11: Dunn's post-hoc test result for LST differences among LCZ pairs using the WUDAPT method.

Dunn's post-hoc test (Bonferroni)								
		LCZ 2	LCZ 5	LCZ 6	LCZ 8	LCZ A	LCZ C	LCZ D
LCZ 5	z	1.95						
	p adjusted	0.72						
LCZ 6	z	2.71	0.78					
	p adjusted	0.10	1.00					
LCZ 8	z	0.97	-1.72	-3.79				
	p adjusted	1.00	1.00	<0.05				
LCZ A	z	15.11	20.51	38.18	32.98			
	p adjusted	<0.05	<0.05	<0.05	<0.05			
LCZ C	z	12.10	14.65	20.72	21.06	-4.78		
	p adjusted	<0.05	<0.05	<0.05	<0.05	<0.05		
LCZ D	z	8.51	9.85	16.27	16.65	-19.83	-8.68	
	p adjusted	<0.05	<0.05	<0.05	<0.05	<0.05	<0.05	
LCZ F	z	8.36	9.69	16.48	16.70	-21.60	-9.29	-0.55
	p adjusted	<0.05	<0.05	<0.05	<0.05	<0.05	<0.05	1.00

Figure 10: LST data distribution for each class of LCZ classification using the WUDAPT method.

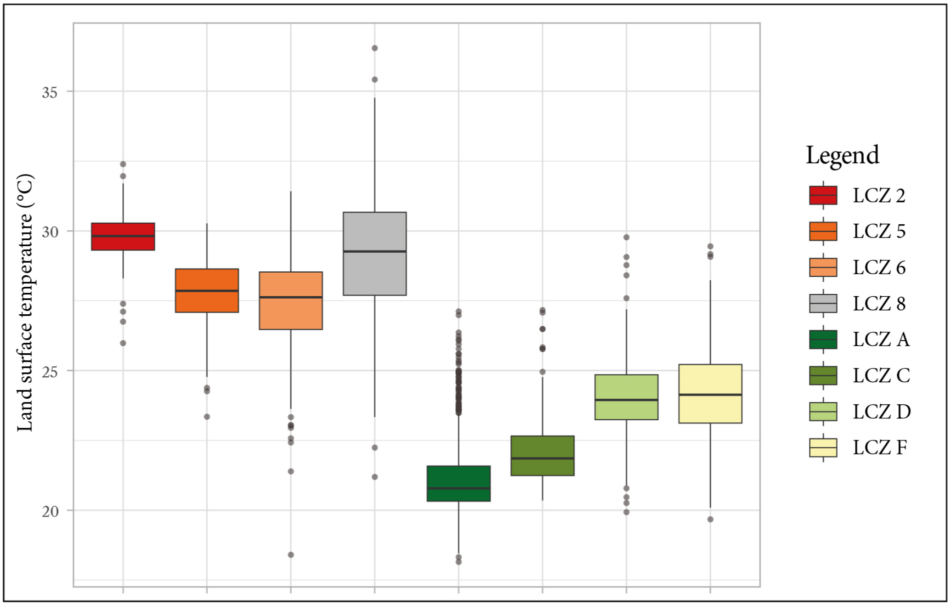

4 DISCUSSION

In this study, we performed two versions of LCZ classification for the city of Ljubljana based on the CA and WUDAPT methods. To our knowledge these represent the first in-depth LCZ classifications for the Ljubljana area following the methodology of Stewart and Oke (2012). The quality of the results was evaluated based on differences in CUHI and LST values across LCZs. It is important to note that both variables allowed us to assess the validity of the classification only in relation to average summer anticyclonic weather conditions. Seasonal and weather-related variations beyond summer anticyclonic conditions were not analysed.

A visual comparison of the LCZ maps (Figure 4, Figure 7) reveals that the results of both methods, which operate in fundamentally different ways, are generally similar. This indicates the robustness of the results in terms of key independent variables that determine the occurrence of LCZs. The main difference between the results for built LCZs (LCZ 1–LCZ 10) is that the WUDAPT method identified four LCZ types that occupy prominent share of the urban area (LCZ 2: compact mid-rise, LCZ 5: open mid-rise, LCZ 6: open low-rise, and LCZ 8: large low-rise), while the CA method identified three prominent types (LCZ 2, LCZ 5, and LCZ 6). Areas classified as LCZ 8 using

WUDAPT method are included within LCZ 6 of the CA classification. The lack of LCZ 8 identification is in line with the LCZ classification result in the study of Quezon City in the Philippines conducted by the authors of the CA method (Estacio et al., 2019). The occurrence of discrepancies in the coverage and number of LCZ types within the same area between remote sensing imagery-based methods and GIS-based or combined methods has already been highlighted in studies of Vienna (Hammerberg et al., 2018) and Brno (Geletič & Lehnert, 2016). In our case, we believe that the primary reason for these discrepancies is the lack of access to GIS layer on anthropogenic heat output, as this variable is critical in distinguishing LCZ 8 from other built LCZ types. The same applies to LCZ 10 (heavy industry) (Stewart & Oke, 2012).

The Kruskal-Wallis test indicated that the medians of LCZs derived from both classification methods differ significantly in relation to CUHI. According to the results of Dunn's post-hoc test, considering CUHI, the medians of most urban LCZ pairs differ significantly. One exception in both classification methods is the relationship between LCZ 2 and LCZ 5. We speculate that a potential reason for this could be the specific urban morphology of Ljubljana, as the city lacks extensive apartment block neighbourhoods commonly found in other larger European cities. This may inhibit the development of a distinct thermal regime. Although the differences in CUHI intensity between the two classes in both classification methods were not statistically significant, boxplots (Figure 5 and Figure 9) show clearly visible gaps between the interquartile ranges on the ordinate axis, suggesting notable differences in intensity between LCZ 2 and LCZ 5. For the WUDAPT classification method, differences were also not statistically significant in the cases of LCZ 2-LCZ 8 and LCZ 5-LCZ 8. Considering the dynamics of CUHI in Ljubljana, where the phenomenon is most intense in the city centre and industrial or commercial areas (Ogrin et al., 2023), substantial differences between LCZ 2 and LCZ 8 cannot reasonably be expected.

Using both classification methods, we identified a methodological limitation in the creation of the CUHI intensity layer in the study by Ogrin et al. (2023). The authors generated the CUHI layer through spatial interpolation of point measurements using the Ordinary Kriging method. Due to the lower density of measurement sites in forested areas and their specific spatial distribution, higher CUHI intensity values were assigned to forested areas compared to grasslands. This is generally inconsistent with the typical thermal relationships between forested and grassland surfaces (Shen et al., 2017). As a result, we cannot fully trust the findings on statistically significant differences of CUHI between LCZ types due to this constraint of the input data. In fact, it would have been most appropriate to use CUHI point measurement data from Ogrin et al. (2023) instead of a raster layer. However, the available point data were insufficient to achieve a satisfactory sample size.

The Kruskal-Wallis rank sum test showed that the medians of LCZs derived from both classification methods also differ significantly in relation to LST. Using the CA method, only the medians of LCZ 2 and LCZ 5 did not differ significantly. For the

WUDAPT classification method, statistically significant differences among built LCZ types were observed only between the medians of LCZ 6 and LCZ 8. This suggests that, from a statistical perspective, spatial differences in LST between LCZ types are small.

The WUDAPT classification method produced a highly robust result in terms of distinguishing between predominantly built-up and predominantly natural LCZs (Figure 8). The F1 score for LCZ 5 was less than 0.2, supporting the hypothesis that identifying this type of LCZ is challenging due to the specific morphological characteristics of the city. The overall classification accuracy (OA = 0.76) is comparable to the quality of classifications for nearby cities (e.g., Zagreb 0.43–0.81; Novi Sad 0.81; Vienna 0.59; Milan 0.35–0.72) (Demuzere et al., 2021). While the results are comparable, they also indicate that further improvements to the classification would be beneficial in the future. A comparison of urban LCZ types in Ljubljana, Zagreb, and Novi Sad reveals that all three cities predominantly consist of LCZ 2, LCZ 5, and LCZ 6. However, the main difference is that Ljubljana is the only one of the three cities without LCZ 3 (compact low-rise) (Demuzere et al., 2021). Alternatively to the WUDAPT approach, Milošević et al. (2022) conducted a classification for Novi Sad following the methodology of Lelovics et al. (2014). In this classification, the authors again identified patterns similar to those observed in Ljubljana. However, they additionally identified LCZ 10, which was absent in both of our classifications.

As the focus of the study was primarily on built LCZs, due to the higher population density and presence of human activities, differences among predominantly natural LCZs (LCZ A–LCZ G) were not given special attention. Another reason for this is that forested areas and water bodies are the only classes that remain relatively stable over time, whereas the use of agricultural land changes on a yearly basis.

Based on the thorough evaluation, the selection of the most appropriate classification had to be made. While both classifications provided similar results, using the WUDAPT classification method commercial and industrial areas were classified as LCZ 8 (Large low-rise). These parts of the city are known to be among the areas with the highest LST (Komac et al., 2016), air temperature and CUHI intensity (Ogrin et al., 2023), and we therefore find this classification to be more representative and applicable, despite confirming fewer differences in LST and CUHI between LCZs with statistical methods compared to the CA classification method.

In LCZ 2 (Compact mid-rise) of WUDAPT classification, we primarily include the central part of the city of Ljubljana, which predominantly consists of historical architecture that was built prior to the Second World War (the area bounded by Castle Hill, Tivoli Park, Tivoli Road, and Aškerčeva Road). In LCZ 5 (Open mid-rise), we include the apartment block neighbourhoods that were identified (the neighbourhood of apartment blocks extending from the north towards the city centre along Celovška Street, the Novo Brdo neighbourhood, the BS neighbourhood, the Savsko neighbourhood, and others). LCZ 6 (Open low-rise) is the most prevalent and consists mainly of residential areas with houses of no more than two floors (e.g., the Rožna Dolina district, the Murgle district, the

Šiška district, parts of the Kodeljevo district, and others). LCZ 8 (Large low-rise) is represented by BTC City Ljubljana, the Šiška Industrial Zone, the Rudnik Shopping District, the Stegne Industrial Zones, and others. As mentioned, among the predominantly natural LCZ types, LCZ A (Dense trees) is worth noting, as it consists of forests overgrowing Rožnik Hill, Castle Hill, Golovec Hill, and several other peripheral areas of our study area.

By conducting this study we developed a microclimatological classification of Ljubljana which enables standardised urban weather and climate research (Wang, Wang, et al., 2024). The classification can be the basis for continuation of UHI studies and development of new study fields, such us outdoor human thermal comfort (Cao et al., 2022; Lam et al., 2023) and air humidity characteristics (Dunjić et al., 2021; Yang et al., 2020). It can be also useful as an input for regional climate models (Ribeiro et al., 2021; Zhao et al., 2024), building energy consumption studies (Kotharkar et al., 2022; Tian et al., 2024) and urban design and planning (He et al., 2024; Wang, Cai, et al., 2024). Despite classification's multidisciplinary applicability, one needs to be aware of the fact that although the term "climate" is included in the classification's name, the delineation of LCZs is exclusively based on the morphological division of the city and is not derived from any meteorological measurements. Moreover, LCZs do not predefine the type of urban climate but provide a sound basis for the studies in the aforementioned fields. According to Stewart and Oke (2012), each LCZ is characterised by a distinct thermal regime, which is most pronounced over dry surfaces on calm, clear nights and in areas with simple topography. While differences in air temperature and other meteorological variables are often observable, the classification alone does not permit the inference of general urban climate characteristics (Huang et al., 2023).

Although the LCZ classification of Ljubljana strictly adheres to the framework established by Stewart and Oke (2012) and has been both quantitatively and qualitatively evaluated, there remains scope for future refinement and further assessment. Our study was constrained by a lack of data for two crucial spatial variables: surface admittance and anthropogenic heat output. The absence of certain explanatory variables is a common limitation in similar studies (Lehnert et al., 2021), raising the question of whether the methodological framework should be redefined and optimised to facilitate greater accessibility to the necessary data. Despite utilising the most up-to-date datasets available for the development of spatial input data, some sources, such as LiDAR, were nearly a decade old. Consequently, the results may not fully reflect the current state of LCZ distribution and would benefit from future updates. As predominantly natural LCZs were not the primary focus of this study due to the aforementioned limitations, future research should place greater emphasis on these areas of the city. Moreover, other advanced classification methods, such as neural networks and random forests (Cui et al., 2022), have yet to be explored. Additionally, the classification was quantitatively evaluated solely under "ideal" weather conditions conducive to the formation of the summer UHI, leaving its applicability under other weather conditions and seasons to be further investigated.

5 CONCLUSION

This study aimed to develop the classification of LCZs in Ljubljana to enable standardised research on urban weather, climate, and various other scientific disciplines. We produced spatial data layers necessary for the classification (G1), classified the LCZs of Ljubljana using the CA and WUDAPT methods (G2 & G3), and evaluated both classifications based on the spatial variability of CUHI, LST, and expert judgement (G4). The classification generated using the WUDAPT method was recognised as more suitable and useful for future research, as it enables a substantial explanation of the quantitative differences in the intensity of summer UHI and LST. Furthermore, this method allowed us to identify large low-rise (LCZ 8) as a distinct type, encompassing industrial zones and large shopping centres. This was not the case with the CA method. Using the WUDAPT method, we identified four predominantly built-up and five predominantly natural LCZs.

Acknowledgments

The authors sincerely thank Dr Estacio and his colleagues for kindly providing us with the Cellular Automata tool, which was a fundamental precondition for this study.

References

Allen, R. G., Tasumi, M., & Trezza, R. (2002). *SEBAL (Surface Energy Balance Algorithms for Land)-Advanced training and user's manual-Idaho implementation, version 1.0*. https://posmet.ufv.br/wp-content/uploads/2017/04/MET-479-Waters-et-al-SEBAL.pdf

Assaf, G., & Assaad, R. H. (2024). Modeling the impact of land use/land cover (LULC) factors on diurnal and nocturnal Urban Heat Island (UHI) intensities using spatial regression models. *Urban Climate*, *55*, 101971. https://doi.org/10.1016/j.uclim.2024.101971

Avdan, U., & Jovanovska, G. (2016). Algorithm for automated mapping of land surface temperature using LANDSAT 8 Satellite Data. *Journal of Sensors*, *2016*, 1480307. https://doi.org/10.1155/2016/1480307

Cao, Q., Huang, H., Hong, Y., Huang, X., Wang, S., Wang, L., & Wang, L. (2022). Modeling intra-urban differences in thermal environments and heat stress based on local climate zones in central Wuhan. *Building and Environment*, *225*, 109625. https://doi.org/10.1016/j.buildenv.2022.109625

Chander, G., & Markham, B. (2003). Revised Landsat-5 TM radiometric calibration procedures and postcalibration dynamic ranges. *IEEE Transactions on Geoscience and Remote Sensing*, *41*(11), 2674–2677. https://doi.org/10.1109/TGRS.2003.818464

Chicco, D., & Jurman, G. (2020). The advantages of the Matthews correlation coefficient (MCC) over F1 score and accuracy in binary classification evaluation. *BMC Genomics*, *21*(1), 6. https://doi.org/10.1186/s12864-019-6413-7

Chien-Ta, C., Chia-Tse, H., Jyh-Dong, L., & Po-Hsun, S. (2015). Application of a decision tree method with a spatiotemporal object database for pavement maintenance and management. *Journal of Marine Science and Technology*, *23*(3), 302–307. https://doi.org/10.6119/JMST-014-0327-5

Ciglič, R., & Komac, B. (2014). Urban heat island atlas: A web tool for the determination and mitigation of urban heat island effects. *Geographia Polonica*, *87*(4), 587–591.

Cui, S., Wang, X., Yang, X., Hu, L., Jiang, Z., & Feng, Z. (2022). Mapping local climate zones in the urban environment: The optimal combination of data source and classifier. *Sensors*, *22*(17), 6407. https://doi.org/10.3390/s22176407

Davenport, A. G., Grimmond, S., Oke, T., & Wieringa, J. (2000). Estimating the roughness of cities and sheltered country. *15th Conference on Probability and Statistics in the Atmospheric Sciences/12th Conference on Applied Climatology, Ashville, NC, American Meteorological Society*, 96–99.

Demuzere, M., Kittner, J., & Bechtel, B. (2021). LCZ generator: A web application to create local climate zone maps. *Frontiers in Environmental Science*, *9*, 637455. https://doi.org/10.3389/fenvs.2021.637455

Demuzere, M., Kittner, J., Martilli, A., Mills, G., Moede, C., Stewart, I. D., van Vliet, J., & Bechtel, B. (2022). A global map of local climate zones to support earth system modelling and urban-scale environmental science. *Earth System Science Data*, *14*(8), 3835–3873. https://doi.org/10.5194/essd-14-3835-2022

Dunjić, J., Milošević, D., Kojić, M., Savić, S., Lužanin, Z., Šećerov, I., & Arsenović, D. (2021). Air humidity characteristics in "local climate zones" of Novi Sad (Serbia) based on long-term data. *ISPRS International Journal of Geo-Information*, *10*(12), 810. https://doi.org/10.3390/ijgi10120810

Estacio, I., Babaan, J., Pecson, N. J., Blanco, A. C., Escoto, J. E., & Alcantara, C. K. (2019). GIS-based mapping of local climate zones using fuzzy logic and cellular automata. *International Archives of the Photogrammetry, Remote Sensing and Spatial Information Sciences*, *XLII-4/W19*, 199–206. https://doi.org/10.5194/isprs-archives-XLII-4-W19-199-2019

Geletič, J., & Lehnert, M. (2016). GIS-based delineation of local climate zones: The case of medium-sized Central European cities. *Moravian Geographical Reports*, *24*(3), 2–12. https://doi.org/doi:10.1515/mgr-2016-0012

Generalization of classified raster imagery—ArcMap | Documentation. (n.d.). Retrieved 17 January 2025, from https://desktop.arcgis.com/en/arcmap/latest/tools/spatial-analyst-toolbox/generalization-of-classified-raster-imagery.htm

Goward, S. N., Markham, B., Dye, D. G., Dulaney, W., & Yang, J. (1991). Normalized difference vegetation index measurements from the advanced very high resolution radiometer. *Remote Sensing of Environment*, *35*(2), 257–277. https://doi.org/10.1016/0034-4257(91)90017-Z

Hammerberg, K., Brousse, O., Martilli, A., & Mahdavi, A. (2018). Implications of employing detailed urban canopy parameters for mesoscale climate modelling: A comparison between WUDAPT and GIS databases over Vienna, Austria. *International Journal of Climatology*, *38*(S1), e1241–e1257. https://doi.org/10.1002/joc.5447

Hammond, D. S., Chapman, L., & Thornes, J. E. (2012). Roughness length estimation along road transects using airborne LIDAR data. *Meteorological Applications*, *19*(4), 420–426. https://doi.org/10.1002/met.273

He, B. J., Fu, X., Zhao, Z., Chen, P., Sharifi, A., & Li, H. (2024). Capability of LCZ scheme to differentiate urban thermal environments in five megacities of China: Implications for integrating LCZ system into heat-resilient planning and design. *IEEE Journal of Selected Topics in Applied Earth Observations and Remote Sensing*, *17*, 18800–18817. https://doi.org/10.1109/JSTARS.2024.3469241

Hu, M., Zhang, K., Nguyen, Q., & Tasdizen, T. (2023). The effects of passive design on indoor thermal comfort and energy savings for residential buildings in hot climates: A systematic review. *Urban Climate*, *49*, 101466. https://doi.org/10.1016/j.uclim.2023.101466

Huang, F., Jiang, S., Zhan, W., Bechtel, B., Liu, Z., Demuzere, M., Huang, Y., Xu, Y., Ma, L., Xia, W., Quan, J., Jiang, L., Lai, J., Wang, C., Kong, F., Du, H., Miao, S., Chen, Y., & Chen, J. (2023). Mapping local climate zones for cities: A large review. *Remote Sensing of Environment*, *292*, 113573. https://doi.org/10.1016/j.rse.2023.113573

Jernej, S. (2000). *Analiza klime Ljubljane*. Inštitut za geografijo Karl-Franzens Univerze.

Kim, M., Jeong, D., & Kim, Y. (2021). Local climate zone classification using a multi-scale, multi-level attention network. *ISPRS Journal of Photogrammetry and Remote Sensing*, *181*, 345–366. https://doi.org/10.1016/j.isprsjprs.2021.09.015

Komac, B., Ciglič, R., Loose, A., Pavšek, M., Čermelj, S., Oštir, K., Kokalj, Ž., & Topole, M. (2016). Urban heat island in the Ljubljana city. In F. Musco (Ed.), *Counteracting Urban Heat Island Effects in a Global Climate Change Scenario* (pp. 323–344). Springer International Publishing.

Kotharkar, R., Ghosh, A., Kapoor, S., & Reddy, D. G. K. (2022). Approach to local climate zone based energy consumption assessment in an Indian city. *Energy and Buildings*, *259*, 111835. https://doi.org/10.1016/j.enbuild.2022.111835

Lam, C. K. C., Shooshtarian, S., & Kenawy, I. (2023). Assessment of urban physical features on summer thermal perceptions using the local climate zone classification. *Building and Environment*, *236*, 110265. https://doi.org/10.1016/j.buildenv.2023.110265

Lehnert, M., Geletič, J., Husák, J., & Vysoudil, M. (2015). Urban field classification by "local climate zones" in a medium-sized Central European city: The case of

Olomouc (Czech Republic). *Theoretical and Applied Climatology*, *122*(3), 531–541. https://doi.org/10.1007/s00704-014-1309-6

Lehnert, M., Savić, S., Milošević, D., Dunjić, J., & Geletič, J. (2021). Mapping local climate zones and their applications in European urban environments: a systematic literature review and future development trends. *ISPRS International Journal of Geo-Information*, *10*(4), 260. https://doi.org/10.3390/ijgi10040260

Lelovics, E., Unger, J., Gál, T., & Gál, C. (2014). Design of an urban monitoring network based on Local Climate Zone mapping and temperature pattern modelling. *Climate Research*, *60*(1), 51–62. https://doi.org/10.3354/cr01220

MAFF [Ministry of Agriculture, Forestry and Food]. (2023). *Grafični podatki RABA za celo Slovenijo* [Spatial data]. https://rkg.gov.si/vstop/

McKnight, P. E., & Najab, J. (2010). Kruskal-Wallis Test. In I. B. Weiner & W. E. Craighead (Eds.), *The corsini encyclopedia of psychology*. John Wiley & Sons.

Mills, G., Bechtel, B., Ching, J., See, L., Feddema, J., Foley, M., Alexander, P., & O'Connor, M. (2015). *An introduction to the WUDAPT project*. 9th International Conference on Urban Climates.

Milošević, D., Savić, S., Kresoja, M., Lužanin, Z., Šećerov, I., Arsenović, D., Dunjić, J., & Matzarakis, A. (2022). Analysis of air temperature dynamics in the "local climate zones" of Novi Sad (Serbia) based on long-term database from an urban meteorological network. *International Journal of Biometeorology*, *66*(2), 371–384. https://doi.org/10.1007/s00484-020-02058-w

Mohite, S., & Surawar, M. (2024). Assessing pedestrian thermal comfort to improve walkability in the urban tropical environment of Nagpur city. *Geographica Pannonica*, *28*(1), 71–84. https://doi.org/10.5937/gp28-48166

Ogrin, D. (2015). Long-term air temperature changes in Ljubljana (Slovenia) in comparison to Trieste (Italy) and Zagreb (Croatia). *Moravian Geographical Reports*, *23*(3), 17–26. https://doi.org/10.1515/mgr-2015-0014

Ogrin, D., & Krevs, M. (2015). Assessing urban heat island impact on long-term trends of air temperatures in Ljubljana. *Dela*, *2015*(43), 41–59. https://doi.org/10.4312/dela.43.3.41-59

Ogrin, M., Lampič, B., Svetlin, D., Štaut, L., & Stefanovski, S. (2022). *Toplotni otok mesta Ljubljana, zaključno poročilo (neobjavljeno)*. UL FF.

Ogrin, M., Svetlin, D., Stefanovski, S., & Lampič, B. (2023). Assessment of winter urban heat island in Ljubljana, Slovenia. *Meteorology*, *2*(2), 222–238. https://doi.org/10.3390/meteorology2020014

Oke, T. R. (2002). *Boundary layer climates* (2nd ed). Routledge. https://doi.org/10.4324/9780203407219

Olofsson, P., Foody, G. M., Herold, M., Stehman, S. V., Woodcock, C. E., & Wulder, M. A. (2014). Good practices for estimating area and assessing accuracy of land change. *Remote Sensing of Environment*, *148*, 42–57. https://doi.org/10.1016/j.rse.2014.02.015

Pipenbaher, N., Ivajnšič, D., Žiberna, Igor, Donša, D., Kaligarič, M., Škornik, S., Kajfež Bogataj, L., Črepinšek, Z., & Grujić, V. J. (2020). Letna dinamika pojava mestnega toplotnega otoka v malem urbanem sistemu. *Revija Za Geografijo*, *15*(2), 91–104.

Qian, S., Peng, T., He, R., Chen, J., Zhang, X., Nazir, M. S., & Zhang, C. (2025). A novel ensemble framework based on intelligent weight optimization and multi-model fusion for air quality index prediction. *Urban Climate*, *59*, 102233. https://doi.org/10.1016/j.uclim.2024.102233

Qiu, C., Mou, L., Schmitt, M., & Zhu, X. X. (2019). Local climate zone-based urban land cover classification from multi-seasonal Sentinel-2 images with a recurrent residual network. *ISPRS Journal of Photogrammetry and Remote Sensing*, *154*, 151–162. https://doi.org/10.1016/j.isprsjprs.2019.05.004

Ribeiro, I., Martilli, A., Falls, M., Zonato, A., & Villalba, G. (2021). Highly resolved WRF-BEP/BEM simulations over Barcelona urban area with LCZ. *Atmospheric Research*, *248*, 105220. https://doi.org/10.1016/j.atmosres.2020.105220

Savić, S., Milošević, D., Lazić, L., Marković, V., Arsenović, D., & Pavić, D. (2013). Classifying urban meteorological stations sites by 'local climate zones': Preliminary results for the city of Novi Sad (Serbia). *Geographica Pannonica*, *17*(3), 60–68. https://doi.org/10.5937/GeoPan1303060S

SEA [Slovenian Environment Agency]. (2011). *Podatki zračnega laserskega skeniranja*. [Prostorski podatki]. https://gis.arso.gov.si/evode/profile.aspx?id=atlas_voda_Lidar%40Arso&initialExtent=402591.76%2C39904.09%2C2.64583

Shen, X., Liu, B., & Lu, X. (2017). Effects of land use/land cover on diurnal temperature range in the temperate grassland region of China. *Science of The Total Environment*, *575*, 1211–1218. https://doi.org/10.1016/j.scitotenv.2016.09.187

Silva, B. B. da, Braga, A. C., Braga, C. C., Oliveira, L. M. M. de, Montenegro, S. M. G. L., & Barbosa Junior, B. (2016). Procedures for calculation of the albedo with OLI-Landsat 8 images: Application to the Brazilian semi-arid. *Revista Brasileira de Engenharia Agrícola e Ambiental*, *20*(1), 3–8. http://dx.doi.org/10.1590/1807-1929/agriambi.v20n1p3-8

SMARS [Surveying and Mapping Authority of the Republic of Slovenia]. (2015). *Digital orthophoto* [Orthophoto]. https://ipi.eprostor.gov.si/jv/?map=jgp

SMARS. (2023a). *Državna topografska karta merila 1: 50 000—Vektorska*. https://eprostor.gov.si/imps/srv/slv/catalog.search#/metadata/ccfeed94-651d-4742-b5b0-ae5a248ea2ca

SMARS. (2023b). *Kataster stavb* [Dataset].

SMARS. (2023c). *Register prostorskih enot* [Dataset].

Sobrino, J. A., Jiménez-Muñoz, J. C., & Paolini, L. (2004). Land surface temperature retrieval from LANDSAT TM 5. *Remote Sensing of Environment*, *90*(4), 434–440. https://doi.org/10.1016/j.rse.2004.02.003

Stewart, I. D., & Oke, T. R. (2012). Local climate zones for urban temperature studies. *Bulletin of the American Meteorological Society*, *93*(12), 1879–1900. https://doi.org/10.1175/BAMS-D-11-00019.1

Tian, X., Zhang, H., Liu, L., Huang, J., Liu, L., & Liu, J. (2024). Establishment of LCZ-based urban building energy consumption dataset in hot and humid subtropical regions through a bottom-up method. *Applied Energy*, *368*, 123491. https://doi.org/10.1016/j.apenergy.2024.123491

Unger, J., Lelovics, E., & Gál, T. (2014). Local climate zone mapping using GIS methods in Szeged. *Hungarian Geographical Bulletin*, *63*(1), 29–41. https://doi.org/10.15201/hungeobull.63.1.3

United Nations. (2019). *World Urbanization Prospects: The 2018 Revision (ST/ESA/SER.A/420).* United Nations.

USGS [U.S. Geological Survey]. (2022). *LC08_L1TP_191028_20220720_20220726_02_T1* [Spatial data]. https://earthexplorer.usgs.gov/

USGS. (2023a). *LC08_L1TP_190028_20230630_20230711_02_T1* [Spatial data]. https://earthexplorer.usgs.gov/

USGS. (2023b). *LC09_L1TP_190028_20230708_20230708_02_T1* [Spatial data]. https://earthexplorer.usgs.gov/

USGS. (2023c). *LC09_L1TP_191028_20230715_20230715_02_T1* [Spatial data]. https://earthexplorer.usgs.gov/

Wang, R., Cai, M., Shi, Y., & Ren, C. (2024). Integration of LCZ to planning strategies. In R. Wang, M. Cai, C. Ren, & Y. Shi (Eds.), *Local Climate Zone Application in Sustainable Urban Development: Experience from East and Southeast Asian High-Density Cities* (pp. 229–241). Springer International Publishing. https://doi.org/10.1007/978-3-031-56168-9_12

Wang, R., Wang, M., Ren, C., Chen, G., Mills, G., & Ching, J. (2024). Mapping local climate zones and its applications at the global scale: A systematic review of the last decade of progress and trend. *Urban Climate*, *57*, 102129. https://doi.org/10.1016/j.uclim.2024.102129

Yang, X., Peng, L. L. H., Chen, Y., Yao, L., & Wang, Q. (2020). Air humidity characteristics of local climate zones: A three-year observational study in Nanjing. *Building and Environment*, *171*, 106661. https://doi.org/10.1016/j.buildenv.2020.106661

Zhao, S., Chen, Y., Zhang, H., & Luo, M. (2024). Impacts of local climate zone mapping quality on urban near-surface air temperature simulation in WRF-UCM. *Sustainable Cities and Society*, *101*, 105171. https://doi.org/10.1016/j.scs.2024.105171

Zhou, X., Okaze, T., Ren, C., Cai, M., Ishida, Y., & Mochida, A. (2020). Mapping local climate zones for a Japanese large city by an extended workflow of WUDAPT Level 0 method. *Urban Climate*, *33*, 100660. https://doi.org/10.1016/j.uclim.2020.100660

Žiberna, I. (2006). Trendi temperatur zraka v Mariboru kot posledica razvoja mestnega toplotnega otoka. *Revija Za Geografijo*, *1*(1), 81–98.

Žiberna, I., & Ivajnšič, D. (2022). Sezonski režim površinskega mestnega toplotnega otoka v Mariboru. In D. Donša, V. J. Grujić, & N. Pipenbaher (Eds.), *Primeri prostorskih analiz vplivov podnebnih sprememb: Monografija v okviru projekta*

Preprečevanje toplotnega stresa v urbanih sistemih v luči podnebnih sprememb (ARRS J7-1822). University of Maribor Press. https://doi.org/10.18690/um.fnm.8.2022

Žiberna, I., Pipenbaher, N., Donša, D., Škornik, S., Kaligarič, M., Bogataj, L. K., Črepinšek, Z., Grujić, V. J., & Ivajnšič, D. (2021). The impact of climate change on urban thermal environment dynamics. *Atmosphere*, *12*(9), 1159. https://doi.org/10.3390/atmos12091159